

## MIT Open Access Articles

*Theoretical study on the HACA chemistry of naphthalenyl radicals and acetylene: The formation of C<sub>12</sub>H<sub>8</sub>, C<sub>14</sub>H<sub>8</sub>, and C<sub>14</sub>H<sub>10</sub> species*

The MIT Faculty has made this article openly available. **Please share** how this access benefits you. Your story matters.

**Citation:** Chu, Te#Chun, Smith, Mica C., Yang, Jeehyun, Liu, Mengjie and Green, William H. 2020. "Theoretical study on the HACA chemistry of naphthalenyl radicals and acetylene: The formation of C<sub>12</sub>H<sub>8</sub>, C<sub>14</sub>H<sub>8</sub>, and C<sub>14</sub>H<sub>10</sub> species." *International Journal of Chemical Kinetics*, 52 (11).

**As Published:** <http://dx.doi.org/10.1002/kin.21397>

**Publisher:** Wiley

**Persistent URL:** <https://hdl.handle.net/1721.1/140914>

**Version:** Author's final manuscript: final author's manuscript post peer review, without publisher's formatting or copy editing

**Terms of use:** Creative Commons Attribution-Noncommercial-Share Alike



# Theoretical Study on the HACA Chemistry of Naphthalenyl Radicals and Acetylene: the formation of $C_{12}H_8$ , $C_{14}H_8$ , and $C_{14}H_{10}$ species

*Te-Chun Chu<sup>a</sup>, Mica C. Smith<sup>a</sup>, Jeehyun Yang<sup>b</sup>, Mengjie Liu<sup>a</sup>, William H. Green<sup>a,\*</sup>*

<sup>a</sup>Department of Chemical Engineering, Massachusetts Institute of Technology, 77 Massachusetts Ave., Cambridge, MA 02139, United States of America

<sup>b</sup>Department of Earth, Atmospheric, and Planetary Sciences, Massachusetts Institute of Technology, 77 Massachusetts Ave., Cambridge, Massachusetts 01239, United States

E-mail: whgreen@mit.edu

## Abstract

The Hydrogen-Abstraction- $C_2H_2$ -Addition (HACA) chemistry of naphthalenyl radicals has been studied extensively, but there is a significant discrepancy in product distributions reported or predicted in literature regarding appearance of  $C_{14}H_8$  and  $C_{14}H_{10}$  species. Starting from ab-initio calculations, a comprehensive theoretical model describing the HACA chemistry of both 1- and 2-naphthalenyl radicals is generated. Pressure-dependent kinetics are considered in the  $C_{12}H_9$ ,  $C_{14}H_9$ , and  $C_{14}H_{11}$  potential energy surfaces (PES) including formally direct well-skipping pathways. On the  $C_{12}H_9$  PES, reaction pathways were found connecting two entry points: 1-naphthalenyl ( $1-C_{10}H_7$ ) + acetylene ( $C_2H_2$ ) and  $2-C_{10}H_7 + C_2H_2$ . A significant amount of acenaphthylene is predicted to be formed from  $2-C_{10}H_7 + C_2H_2$  and the appearance of  $C_{14}H_8$  isomers are predicted in the model simulation, consistent with high-temperature experimental results from Parker et al. At 1500 K,  $1-C_{10}H_7 + C_2H_2$  mostly generates acenaphthylene through a formally direct pathway, which predicted selectivity of 66% at 30 Torr and 56% at 300 Torr. The reaction of  $2-C_{10}H_7$  with  $C_2H_2$  at 1500 K yields 2-ethynynaphthalene as the most dominant product, followed by acenaphthylene mainly generated via isomerization of  $2-C_{10}H_7$  to  $1-C_{10}H_7$ . Both the  $1-C_{10}H_7$  and  $2-C_{10}H_7$  reactions with  $C_2H_2$  form some  $C_{14}H_8$  products, but negligible phenanthrene and anthracene formation is predicted at 1500 K. A rate-of-production (ROP) analysis reveals that  $C_{14}H_8$  formation is strongly affected by the rates of H-abstraction from acenaphthylene, 1-ethynynaphthalene, and 2-ethynynaphthalene, so the kinetics of these reactions are accurately calculated at the high level G3(MP2,CC)//B3LYP/6-311G\*\* level of theory. At intermediate temperatures like 800 K, acenaphthylene + H are the leading bimolecular

This is the author manuscript accepted for publication and has undergone full peer review but has not been through the copyediting, typesetting, pagination and proofreading process, which may lead to differences between this version and the [Version of Record](#). Please cite this article as [doi: 10.1002/kin.21397](https://doi.org/10.1002/kin.21397).

This article is protected by copyright. All rights reserved.

products of  $1\text{-C}_{10}\text{H}_7 + \text{C}_2\text{H}_2$ , and 1-acenaphthenyl radical is the most abundant  $\text{C}_{12}\text{H}_9$  isomer due to its stability. The predicted product distribution of  $2\text{-C}_{10}\text{H}_7 + \text{C}_2\text{H}_2$  at 800 K, in contrast to the results of Parker et al, is predicted to consist primarily of species containing three fused benzene rings - e.g., phenanthrene and anthracene - as the leading products, indicating HACA chemistry is valid from two to three ring PAHs under some conditions. Further experiments are needed for validation.

## Introduction

Polycyclic aromatic hydrocarbons (PAH) commonly appear in various chemical processes and in flames, especially from incomplete combustion of species like methane<sup>1-4</sup>, ethene<sup>5-7</sup>, and benzene<sup>8-11</sup>. The formation of PAH is normally viewed as an undesired by-product, since it reduces the yield of desired products, and the subsequent soot formation<sup>12-15</sup> has negative effects on human health<sup>16</sup>, climate change<sup>17</sup>, and process efficiency<sup>18</sup>. It is necessary to investigate the PAH formation fundamentally from the angle of both experiments and models, and to successfully apply the knowledge gained to optimize current chemical technology.

Starting from benzene, the simplest aromatic species, and its radical form, phenyl radical, reactions with unsaturated hydrocarbons can lead to ring cyclization to generate PAH. Hydrogen-abstraction- $\text{C}_2\text{H}_2$ -addition (HACA) routes<sup>11,19-23</sup> involving two  $\text{C}_2\text{H}_2$  additions to form an additional six-member aromatic ring are among the most studied and important pathways. The HACA extension from the first to second ring leading to naphthalene has been widely studied experimentally<sup>24-27</sup> and theoretically<sup>28-31</sup>, and it has been recognized as the dominant pathway. However, further aromatic ring addition from naphthalene to phenanthrene (PTR) and anthracene (ANT) remains ambiguous at different temperature conditions. Utilizing high  $\text{C}_2\text{H}_2$  concentrations in a pyrolysis reactor, Parker et al. used a reflectron time-of-flight mass spectrometer (Re-TOF) to measure product formation in the reactions of both 1-naphthalenyl radical ( $1\text{-C}_{10}\text{H}_7$ ) +  $\text{C}_2\text{H}_2$  and 2-naphthalenyl radical ( $2\text{-C}_{10}\text{H}_7$ ) +  $\text{C}_2\text{H}_2$ <sup>32</sup>. At combustion-like temperatures up to 1500 K, no PTR or ANT were detected as peaks in the mass spectra; instead, signals corresponding to  $\text{C}_{14}\text{H}_8$  isomers were detected, which implies hydrogen atom elimination dominated over the cyclization of  $\text{C}_{14}\text{H}_{11}$  adducts formed by the addition of two  $\text{C}_2\text{H}_2$  molecules. In the experiments of Parker et al., acenaphthylene (ACN) was observed as an important product in the reactions of both naphthalenyl radicals with  $\text{C}_2\text{H}_2$ . The observation is not surprising for  $1\text{-C}_{10}\text{H}_7 + \text{C}_2\text{H}_2$ , because the stability of ACN, a H-loss product after the first  $\text{C}_2\text{H}_2$  addition, suggests that its formation is favored over the second  $\text{C}_2\text{H}_2$  addition. However, no reasonable pathway for ACN formation from  $2\text{-C}_{10}\text{H}_7 + \text{C}_2\text{H}_2$  had been proposed in theoretical works<sup>28,33,34</sup> to the best of our knowledge. Parker et al. did not detect PTR or ANT formation in the temperature range from room temperature to 1500 K.<sup>32</sup> This conclusion contrasts with modeling results reported by Kislov et al.<sup>34</sup>, where both PTR and ANT account for significant product yields of  $2\text{-C}_{10}\text{H}_7 + \text{C}_2\text{H}_2$  from room temperature up to 900 K. In the present work, a comprehensive model is developed based on the calculations of Kislov et al. and Liu et al.<sup>28,34</sup>, with the addition of several updated and newly calculated reaction pathways. The model is adaptable to a wide range of temperatures and pressures for general modeling purposes. The main goal of this detailed pressure-dependent model is to resolve discrepancies about ACN formation from  $2\text{-C}_{10}\text{H}_7 + \text{C}_2\text{H}_2$ , the appearance of  $\text{C}_{14}\text{H}_8$  products at high temperature, and PTR/ANT formation at low/intermediate temperatures.

## Theoretical methods

### $C_{12}H_9$ and $C_{14}H_{11}$ Potential Energy Surface Calculations

The HACA routes of 1- and 2-naphthalenyl radicals (1- $C_{10}H_7$  and 2- $C_{10}H_7$ ) were explored by Kislov et al.<sup>34</sup> at the G3(MP2,CC)//B3LYP/6-311G\*\* level of theory. The routes include (1) reactions on the  $C_{12}H_9$  potential energy surface (PES) corresponding to first acetylene ( $C_2H_2$ ) addition; (2) reactions on the  $C_{14}H_{11}$  PES related to the Bittner-Howard<sup>11</sup> and Modified Frenklach<sup>22,23</sup> routes of second  $C_2H_2$  addition to six  $C_{12}H_9$  isomers; and (3) some important channels on the  $C_{14}H_9$  PES associated with the Frenklach<sup>19-21</sup> route involving the addition of a second  $C_2H_2$  to  $C_{12}H_7$  isomers generated by H-abstraction from 1-ethynynaphthalene (1-ETN) or 2-ethynynaphthalene (2-ETN). Extensive quantum chemistry information including optimized geometry was provided in Kislov et al.'s supporting information for all reported species and transition states, but their supporting information omitted some data on hindered rotors and some information on the  $C_{14}H_9$  PES. In 2019, Frenklach et al.<sup>33</sup> revisited the  $C_{12}H_9$  PES using the same level of theory, updating with some revised energies for local minima and results of 1-D hindered-rotors for computing partition functions for certain stable molecules and transition states.

In the present work, five additional  $C_{12}H_9$  isomers along with twelve new transition states are newly added to the  $C_{12}H_9$  PES, shown in Figure 1. The naming scheme here follows Kislov et al.'s conventions.<sup>34</sup> In the work by Kislov et al., two separate networks on the  $C_{12}H_9$  PES starting from 1- $C_{10}H_7$  and 2- $C_{10}H_7$  were reported as two independent systems.<sup>33,34</sup> Here, with the newly calculated  $C_{12}H_9$  isomer named "N-shared" the two  $C_{12}H_9$  networks are connected; the impact of this change on kinetics and product distribution will be discussed later. Reaction pathways on the  $C_{14}H_{11}$  PES starting from three  $C_{12}H_9$  isomers (1-N2, 1-N7, and 1-N11) originating from 1- $C_{10}H_7$  are presented in Figure 2, and reaction pathways involving three  $C_{12}H_9$  isomers originating from 2- $C_{10}H_7$  (2-N2, 2-N8, 2-N11) reacting with  $C_2H_2$  along with an additional  $C_{14}H_{11}$  isomer, one  $C_{14}H_{10}$  (3-vinylacenaphthylene, ACNV2) + H product, and two transition states are shown in Figure 3. The same level of theory as that used in Kislov et al., G3(MP2,CC)//B3LYP/6-311G\*\*, was used in the calculations presented here, and all the calculations were performed in Gaussian 16<sup>35</sup> and Gaussian 09, except for the rCCSD(T) energy used in the G3(MP2,CC) method which was calculated with Molpro 2015<sup>36-46</sup>. To ensure that the lowest energy conformer has been found and maintain consistency of energy calculations given the newer versions of Gaussian and Molpro used in this work, the geometries and energies of all previously reported stable molecules and transition states on the  $C_{12}H_9$  and  $C_{14}H_{11}$  PESs have been reoptimized and recalculated.

Arkane<sup>47</sup>, a package included in the open-source software Reaction Mechanism Generator (RMG)<sup>48</sup>, was used to calculate phenomenological pressure-dependent rate coefficients  $k(T,P)$  on the  $C_{12}H_9$  and  $C_{14}H_{11}$  PESs. The modified strong collision approximation as implemented by Allen *et al.*<sup>47</sup> is used here to calculate  $k(T,P)$  from the  $C_{12}H_9$  and  $C_{14}H_{11}$  pressure-dependent networks





cyclization forming the radical form of PTR and ANT or  $\beta$ -scission to  $C_{14}H_8$  products. It is important to fully investigate possible reaction pathways on the  $C_{14}H_9$  PES, critical to the Frenklach pathway of naphthalenyl radicals.

Rate coefficients of most elementary reactions on the  $C_{14}H_9$  PES were previously evaluated at the high pressure limit using transition state theory (TST) by Liu et al.<sup>28</sup> at the B3LYP/6-311+G\*\* level of theory. In the present work, using the approach of Allen et al.<sup>47</sup> as implemented in Arkane, the pressure-dependent rate coefficients on the Liu et al.<sup>28</sup> PES were evaluated using thermochemistry properties from the "Aromatics\_1dHR" thermochemistry library and Liu et al.'s TST rate constants, with Lennard-Jones parameters estimated by group additivity to predict collision rates. For each unimolecular product or reactant in the surface, the density of states  $\rho(E)$  of the isomers is approximated by fitting functional groups to specific frequencies. The remaining unspecified degrees of freedom, are fit to the heat capacity data of the above-mentioned thermochemistry data in NASA polynomials form. During this calculation, the translational and rotational modes are removed and handled separately.<sup>47</sup> Microcanonical rate coefficients,  $k(E)$ , were estimated from the high-pressure-limit rate coefficients  $k(T)$  and  $\rho(E)$  using the inverse Laplace transform (ILT). For the modified Arrhenius form of  $k(T)$ , there is an exact ILT formula for positive activation energies and  $n > -0.5$ . When the exact formula was not available or has numerical difficulties, the inverse Laplace transform was evaluated numerically. The pressure-dependent rate coefficients,  $k(T,P)$ , were then computed using the modified strong collision approximation with at least 250 energy grains spaced less than 0.5 kcal/mol apart. The calculated kinetics include the  $C_2H_2$  addition to the  $C_{12}H_7$  radicals formed by H-abstraction or H-elimination of 1-ETN and 2-ETN, following the pathways given by Liu et al.<sup>28</sup> This computational method for computing  $k(T,P)$  from literature  $k_\infty(T)$ 's was previously described by Chu et al.<sup>4</sup>

In this work, pressure-dependent reactions of  $C_{12}H_7$  radicals from ACN with  $C_2H_2$  on the  $C_{14}H_9$  PES are considered in detail for the first time. There are four  $C_{12}H_7$  radicals: N1-CS38, N1-CS39, N1-CS40, and N1-CS41, and the corresponding  $C_{14}H_9$  PES is presented in Figure 4. All the stable molecules and transition states are calculated at the G3(MP2,CC)//B3LYP/6-311G\*\* level of theory with the RRHO + 1-D hindered-rotor approximation. Similar to the treatment for the  $C_{12}H_9$  and  $C_{14}H_{11}$  PESs, Arkane<sup>47</sup> with the modified strong collision approximation was used to calculate  $k(T,P)$  for reactions in this new network and the rates are included in the final model.

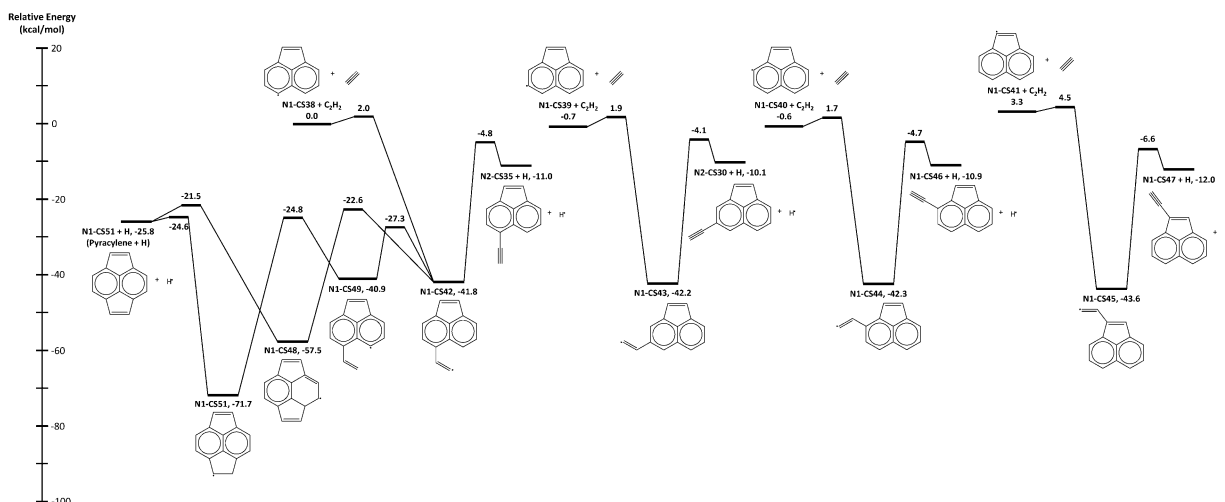


**Figure 4.**  $C_{14}H_9$  potential energy surface calculated at the G3(MP2,CC)//B3LYP/6-311G\*\* level of theory, starting from N1-CS38, N1-CS39, N1-CS40, and N1-CS41 isomers reacting with  $C_2H_2$ . Energies are relative to N1-CS38 +  $C_2H_2$ .

### Combined Naphthalenyl HACA Model

In addition to reactions on the  $C_{12}H_9$ ,  $C_{14}H_9$ , and  $C_{14}H_{11}$  PESs, other reactions such as H-abstraction and radical recombination are important to the naphthalenyl radicals' HACA networks - for example, H-abstraction from 1-ETN, 2-ETN, ACN, 1-vinylnaphthalene (1-VNP), and 2-vinylnaphthalene (2-VNP), and radical recombination between H atom and phenanthrenyl or anthracenyl radicals. The formation of closed-shell species including ANT and PTR involves these reactions which connect species on different PESs. The most important radical is H atom since it is a co-product of all  $\beta$ -scission reactions on the PESs, and highly reactive under most conditions. Under high  $C_2H_2$  concentrations as in Parker et al.'s experiment<sup>32</sup>, we can expect a significant amount of H atom would react with  $C_2H_2$  forming vinyl radical ( $C_2H_3$ ). In this work, the kinetics of 48 important H atom and  $C_2H_3$  radical H-abstraction reactions are calculated at the G3(MP2,CC)//B3LYP/6-311G\*\* level of theory using transition state theory. The Supporting Information includes molecular information of these reactions in Arkane input format, and details of the kinetics will be discussed in a later section. For other reactions in the final mechanism, their rates are less sensitive to the overall product distribution, so the kinetics are estimated by making analogies between small species and large ( $C_{12}$ ,  $C_{14}$ , and up to  $C_{20}$ ) species. For instance, the rate of PTR radical + H  $\rightarrow$  PTR is estimated using the rate of Naphthalenyl radical + H  $\rightarrow$  Naphthalene in literature<sup>52</sup>. The final mechanism reported in Chemkin format includes the reference for each of these reactions.

Given the prevalence of  $C_2H_2$  and  $C_2H_3$  radical in the naphthalenyl HACA system with high  $C_2H_2$  concentration, reactions of  $C_2H_3$  +  $C_2H_2$  leading to the formation of benzene and fulvene cannot be neglected. Using pressure and temperature dependent rate coefficients calculated from the  $C_4H_5$  PES reported by Ribeiro and Mebel using the CCSD(T)-F12//B2PLYPD3 method<sup>53</sup> and the pressure-dependent rate coefficients from Senosiain and Miller on the  $C_6H_7$  PES, which has  $C_6H_7$  isomers, benzene + H, and fulvene + H as products, at the rQCISD(T)/cc-pV $\infty$ Z//B3LYP/6-311++G(d,p) level of theory<sup>54</sup>, these side reactions are included in the final model. Isomerization via direct intramolecular hydrogen transfer between 1-naphthalenyl and 2-naphthalenyl radical was pointed out by Parker et

al.,<sup>32</sup> which was proposed to possibly account for the ACN formation from 2-naphthalenyl radical + C<sub>2</sub>H<sub>2</sub>. This isomerization is considered on the C<sub>10</sub>H<sub>7</sub> PES studied by Mebel et al.<sup>55</sup> and Chu et al.<sup>24</sup>, and on the C<sub>12</sub>H<sub>9</sub> PES between N1-CS12 and N1-CS41 calculated here; the corresponding pressure-dependent rate coefficients are incorporated into the model of this work.

In summary, the final model combined pressure-dependent reaction networks on the C<sub>12</sub>H<sub>9</sub>, C<sub>14</sub>H<sub>9</sub>, and C<sub>14</sub>H<sub>11</sub> PESs with side reactions to comprise a total of 148 species and 624 reactions, and is intended to model naphthalenyl radical + C<sub>2</sub>H<sub>2</sub> reactions at high C<sub>2</sub>H<sub>2</sub> concentrations in pyrolysis conditions without oxygen involved. The Chemkin input file for this model is included in Supporting Information along with each species' adjacency list in the accompanying species dictionary. The naming convention for species on the C<sub>12</sub>H<sub>9</sub> and C<sub>14</sub>H<sub>11</sub> PESs follows that in Kislov et al.'s work<sup>34</sup>; however, since species names starting with a number are not allowed in RMG and Chemkin, the number and suffix are reversed in the Chemkin input file, e.g., 1-N1 is referred to as N1-1. For species on the C<sub>14</sub>H<sub>9</sub> PES, the naming convention follows Liu et al.'s study<sup>28</sup>. Chemical Workbench<sup>56</sup> was used with the final model to simulate various temperature conditions, and to perform the pathway analysis and rate of production (ROP) analysis presented in this work.

## Results & Discussion

### New Reaction Pathways on C<sub>12</sub>H<sub>9</sub> and C<sub>14</sub>H<sub>11</sub> Potential Energy Surfaces

Naphthalene has two positions,  $\alpha$  and  $\beta$ , that can undergo hydrogen abstraction, and the respective radical products are 1-naphthalenyl (1-C<sub>10</sub>H<sub>7</sub>) and 2-naphthalenyl (2-C<sub>10</sub>H<sub>7</sub>) radicals. When C<sub>2</sub>H<sub>2</sub> is attacked by either of these radicals, the resulting adducts and bimolecular products represent two different entry points on the C<sub>12</sub>H<sub>9</sub> PES. In Kislov et al.'s<sup>34</sup> and Frenklach et al.'s<sup>33</sup> calculations, cyclobuta-[a]naphthalene (CB[a]N) + H is the only bimolecular product co-existing on the 1-C<sub>10</sub>H<sub>7</sub> + C<sub>2</sub>H<sub>2</sub> and 2-C<sub>10</sub>H<sub>7</sub> + C<sub>2</sub>H<sub>2</sub> networks, and no consideration was made for common C<sub>12</sub>H<sub>9</sub> isomers shared by the two networks. Therefore, ACN, a bimolecular product on the 1-C<sub>10</sub>H<sub>7</sub> + C<sub>2</sub>H<sub>2</sub> network, should not appear when the reaction starts from 2-C<sub>10</sub>H<sub>7</sub> + C<sub>2</sub>H<sub>2</sub>. However, in Parker's experiments<sup>32</sup>, the mass spectra showed large signals at the mass-to-charge ratio ( $m/z$ ) 152, corresponding to products generated from H-elimination reactions of C<sub>12</sub>H<sub>9</sub> isomers, for both 1-C<sub>10</sub>H<sub>7</sub> + C<sub>2</sub>H<sub>2</sub> and 2-C<sub>10</sub>H<sub>7</sub> + C<sub>2</sub>H<sub>2</sub>. For the 2-C<sub>10</sub>H<sub>7</sub> + C<sub>2</sub>H<sub>2</sub> experiments, the measured photoionization efficiency curves at  $m/z$  152 could be reproduced nicely by a linear combination of the reference PIE curves of 2-ETN and ACN<sup>32</sup>, indicating that ACN accounts for a significant portion of product formation from 2-C<sub>10</sub>H<sub>7</sub> + C<sub>2</sub>H<sub>2</sub>. Parker et al.<sup>32</sup> suggested the intramolecular H-transfer converting 2-C<sub>10</sub>H<sub>7</sub> to 1-C<sub>10</sub>H<sub>7</sub> must be fast to explain the formation of ACN from 2-C<sub>10</sub>H<sub>7</sub> + C<sub>2</sub>H<sub>2</sub>. This process was considered in this work by including the pressure-dependent reactions on the C<sub>10</sub>H<sub>7</sub> PES, including isomerization between 1-C<sub>10</sub>H<sub>7</sub> and 2-C<sub>10</sub>H<sub>7</sub>, from previously reported calculations<sup>24,55</sup>.

As a result of careful consideration of the isomerization between more than 10 isomers on the C<sub>12</sub>H<sub>9</sub> PES, a new local minimum was found connecting the isomers 1-N11 and 2-N8. The new isomer and two connecting TSs were calculated at the same level of theory as the rest of the species on the C<sub>12</sub>H<sub>9</sub> PES. In Figure 1, the new isomer, N-shared, links the left-side species produced from 2-C<sub>10</sub>H<sub>7</sub> + C<sub>2</sub>H<sub>2</sub> to the species on the right produced from 1-C<sub>10</sub>H<sub>7</sub> + C<sub>2</sub>H<sub>2</sub>. The series of reactions

converting 2-C<sub>10</sub>H<sub>7</sub> + C<sub>2</sub>H<sub>2</sub> to 1-C<sub>10</sub>H<sub>7</sub> + C<sub>2</sub>H<sub>2</sub> are summarized in Figure 5; although there are six TSs involved instead of one TS as in the direct intramolecular H-transfer reaction, none of the intermediates or TSs have energies higher than the initial reactants, 2-C<sub>10</sub>H<sub>7</sub> + C<sub>2</sub>H<sub>2</sub>. Furthermore, the pressure-dependent kinetics include well-skipping pathways (or called “formally direct” pathways, i.e. reactions traversing more than one transition state<sup>57-60</sup>) which enable reaction channels forming ACN and 1-C<sub>10</sub>H<sub>7</sub> related isomers like 1-N8 or 1-N11 directly from 2-C<sub>10</sub>H<sub>7</sub> + C<sub>2</sub>H<sub>2</sub> or 2-N8. In the next section, more details about the formation of ACN and its pathways will be given.

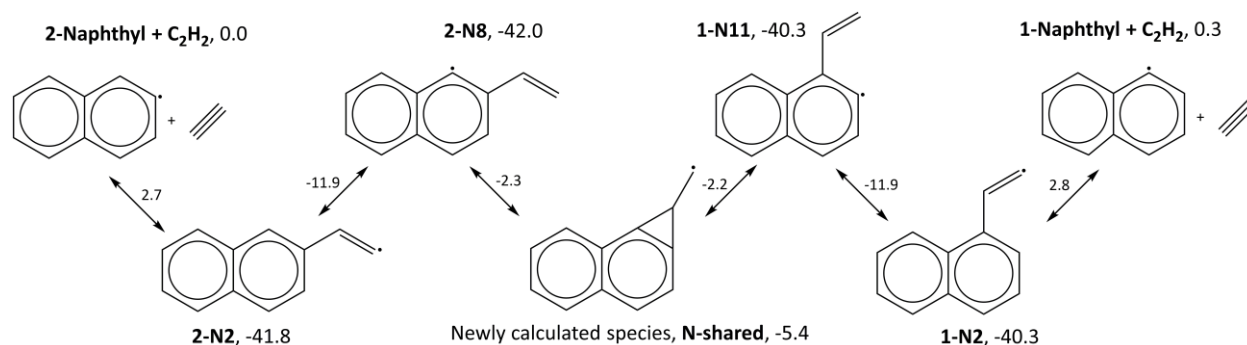


**Figure 5.** Important elementary reactions connecting 1-C<sub>10</sub>H<sub>7</sub> + C<sub>2</sub>H<sub>2</sub> and 2-C<sub>10</sub>H<sub>7</sub> + C<sub>2</sub>H<sub>2</sub> networks. The energy of species is given relative to 2-C<sub>10</sub>H<sub>7</sub> + C<sub>2</sub>H<sub>2</sub> in kcal/mol, and the energy of each TS is shown next to the corresponding arrow.

In addition to the new isomer N-shared implemented on the C<sub>12</sub>H<sub>9</sub> PES, four other new isomers were calculated in this work, as well as the TSs corresponding to reactions connecting them to previously calculated species. These four species, 1-N14, 2-N14, 2-N16, and 2-N17, are resonance-stabilized radicals and so are expected to have relatively low energies. Indeed, their calculated energies are at least 43 kcal/mol more stable than 2-C<sub>10</sub>H<sub>7</sub> + C<sub>2</sub>H<sub>2</sub>. At intermediate temperatures, resonance-stabilized radicals with aromatic rings have been found to have longer lifetimes than other radicals<sup>24</sup>. Optimized geometries for species 1-N14, 2-N16, and 2-N17 were previously reported by Park et al.<sup>61</sup>, and we recalculated them at the G3(MP2,CC)//B3LYP/6-311G\*\* level of theory, whereas to our knowledge 2-N14 has not previously been reported in the literature. On the C<sub>14</sub>H<sub>11</sub> PES, two additional species and two new TSs are considered in this work, shown in Figure 3. ACNV2, which has the same 6,6,5-member ring structure as the stable ACN, has a lower energy than the ethynyl products, and its formation pathway from 2-N9 has been discovered and calculated.

The full mechanism in the Supporting Information contains all the reaction channels from pressure-dependent calculations on the C<sub>12</sub>H<sub>9</sub> PES, as well as two well-skipping pathways that are important to the formation of ACN from 2-C<sub>10</sub>H<sub>7</sub> + C<sub>2</sub>H<sub>2</sub>: 2-N1 + C<sub>2</sub>H<sub>2</sub> (+M) → ACN + H (+M) and 2-N8 (+M) → 1-N11 (+M). The first reaction provides a formally-direct chemically-activated pathway generating ACN from 2-C<sub>10</sub>H<sub>7</sub> + C<sub>2</sub>H<sub>2</sub>, and the second formally-direct reaction passes transiently through the relatively unstable isomer, N-shared, to produce 1-N11 directly from 2-N8, which are both stable with ~40 kcal/mol energy lower than 2-C<sub>10</sub>H<sub>7</sub> + C<sub>2</sub>H<sub>2</sub>. Once 1-N11 is generated, the following reactions on the 1-C<sub>10</sub>H<sub>7</sub> + C<sub>2</sub>H<sub>2</sub> network easily lead to the most stable bimolecular products, ACN + H. Their rate coefficients under various *T*, *P* conditions are listed in Table 1; reaction 2-N1 + C<sub>2</sub>H<sub>2</sub> (+M) → 2-N2 (+M) is included as a reference indicating how fast the direct adduct is

formed in this system. As temperature increases, the kinetics of both reactions become faster; 2-N1 + C<sub>2</sub>H<sub>2</sub> (+M) → ACN + H (+M) is very sensitive to pressure at high temperature conditions, whereas 2-N8 (+M) → 1-N11 (+M) has less significant change in  $k(T, P)$  as pressure increases at high temperature. The rate of 2-N1 + C<sub>2</sub>H<sub>2</sub> (+M) → ACN + H (+M) increases significantly as the temperature rises above 1700 K; however, it is much slower than the rate of 2-N1 + C<sub>2</sub>H<sub>2</sub> (+M) → 2-N2 (+M) at lower temperatures regardless of pressure. Therefore, we expect the reaction 2-N1 + C<sub>2</sub>H<sub>2</sub> (+M) → ACN + H (+M) becomes the dominant pathway forming ACN at extremely high temperatures, and other pathways such as 2-C<sub>10</sub>H<sub>7</sub> isomerization to 1-C<sub>10</sub>H<sub>7</sub> or the multi-step pathway converting 2-N8 to 1-N11 are more important around 1500 K or lower temperatures. The following pathway analysis section will give a complete picture of ACN formation from 2-C<sub>10</sub>H<sub>7</sub> + C<sub>2</sub>H<sub>2</sub>.

**Table 1. Pressure-dependent rate coefficients of important reactions in ACN formation from 2-naphthalenyl + C<sub>2</sub>H<sub>2</sub> on the C<sub>12</sub>H<sub>9</sub> PES.**

Reactions	T (K) / P (atm)	Pressure-dependent rate coefficients, $k(T, P)^a$			
		0.039	0.30	3.3	26.0
2-C <sub>10</sub> H <sub>7</sub> + C <sub>2</sub> H <sub>2</sub> (+M) → 2-N2 (+M)	469	5.61E+10	5.69E+10	5.71E+10	5.71E+10
	651	2.11E+11	2.22E+11	2.24E+11	2.24E+11
	1011	5.16E+11	8.43E+11	1.02E+12	1.05E+12
	1758	5.46E+10	3.04E+11	1.50E+12	3.50E+12
2-C <sub>10</sub> H <sub>7</sub> + C <sub>2</sub> H <sub>2</sub> (+M) → ACN + H (+M)	469	1.80E+02	1.44E-01	4.49E-06	2.12E-10
	651	2.40E+05	7.88E+02	1.09E-01	6.45E-06
	1011	8.36E+08	2.80E+07	5.38E+04	2.09E+01
	1758	2.81E+10	1.20E+10	8.34E+08	9.22E+06
2-N8 (+M) → 1-N11 (+M)	469	1.40E-06	1.39E-06	1.34E-06	1.08E-06
	651	2.31E-01	2.35E-01	2.33E-01	2.16E-01
	1011	1.06E+04	1.55E+04	1.68E+04	1.66E+04
	1758	1.26E+06	1.37E+07	6.02E+07	8.83E+07

<sup>a</sup> Units: s<sup>-1</sup> for unimolecular reactions, cm<sup>3</sup>/(mol\*s) for bimolecular reactions

#### Reactions on C<sub>14</sub>H<sub>9</sub> Potential Energy Surface Including Pyracylene Formation and H-abstraction

Among the three main pathways of HACA chemistry - the Frenklach<sup>19-21</sup>, Bittner-Howard<sup>11</sup>, and Modified Frenklach<sup>22,23</sup> pathways, the Frenklach pathway has been found as the leading route of aromatic ring growth from benzene to naphthalene under high temperature rich-methane conditions<sup>4</sup>. To build a comprehensive model of HACA chemistry valid over the full  $T$  range, all three pathways should be considered. In the case of naphthalenyl radicals, unlike the Bittner-Howard and Modified Frenklach pathways which involve addition of a second C<sub>2</sub>H<sub>2</sub> molecule to the C<sub>12</sub>H<sub>9</sub> isomers formed from the first C<sub>2</sub>H<sub>2</sub> addition, the Frenklach pathway begins with C<sub>12</sub>H<sub>7</sub> radicals, the H-abstraction products of 1-ETN and 2-ETN. The second C<sub>2</sub>H<sub>2</sub> in the Frenklach pathway then adds to the C<sub>12</sub>H<sub>7</sub> radicals on the C<sub>14</sub>H<sub>9</sub> PES followed by cyclization of the third aromatic ring. In addition to 1-ETN and 2-ETN, ACN also may lose an H-atom through H-abstraction, reverse disproportionation, or C-H bond dissociation, and undergo second C<sub>2</sub>H<sub>2</sub> addition on the same C<sub>14</sub>H<sub>9</sub> PES as seen in Figure 4. Although some of the C<sub>12</sub>H<sub>7</sub> radicals rapidly isomerize, there are no common intermediates on the C<sub>14</sub>H<sub>9</sub> PES starting from a radical derived from ACN and the C<sub>14</sub>H<sub>9</sub> PES starting from a radical derived from 1-ETN and 2-ETN, suggesting PTR or ANT cannot be generated directly from a radical formed by

removing an H atom from ACN. However, a stable 6,6,5,5-member ring species, pyracyclene, is expected to be formed from  $C_2H_2$  addition to certain ACN radicals. Based on the CB3-QB3 calculations in the “Aromatics\_1dHR” RMG thermochemistry library<sup>48</sup>, the standard enthalpy of pyracyclene (N1-CS51) formation is at least 15 kcal/mol more stable than any other  $C_{14}H_8$  products studied here. In addition to pyracyclene, other  $C_{14}H_8$  products on the ACN pathway are also thermally favorable because of the 6,6,5-member ring structure.

In Liu et al.’s calculations<sup>28</sup>, the rates of reactions on the  $C_{14}H_9$  PES starting from 1-ETN and 2-ETN were determined assuming the high-pressure limit with transition state theory. With the help of Arkane, these kinetics are converted into pressure-dependent rate coefficients including well-skipping reactions. We also include the reactions on the  $C_{14}H_9$  PES starting from ACN, and the ab-initio calculations are performed at the G3(MP2,CC)//B3LYP/6-311G\*\* level of theory. The new additions to the PES are shown in Figure 4. Four radicals, N1-CS38, N1-CS39, N1-CS40, and N1-CS41, react with  $C_2H_2$  to generate four adducts, N1-CS42, N1-CS43, N1-CS44, N1-CS45. The energy barriers of the reactions fall within 1.2-2.6 kcal/mol, and the adducts are >40 kcal/mol more stable than the reactants. Except for N1-CS41, the reactants have radicals on their benzene ring, so the low barriers and the exothermicities are similar to naphthalenyl radicals +  $C_2H_2$ . N1-CS42 can cyclize to produce another fused ring, because its  $C_2H_2$  group is close to the other benzene ring on its structure. Therefore, both  $\beta$ -scission reactions to ethynyl species and intramolecular ring growth pathways are calculated for the reactions shown in Figure 4. The final product of the pathways is pyracyclene, and it is the most stable  $C_{14}H_8$  product as predicted from the enthalpy data.

H-abstraction reactions are undoubtedly highly important to the reactions in the Frenklach pathway. In Mebel et al.’s work<sup>62</sup>, the transition state for H-abstraction from phenylacetylene is the highest barrier in the whole phenyl radical HACA network. Liu et al. calculated the H atom H-abstraction kinetics for 1-ETN and 2-ETN at the B3LYP/6-311+G\*\* level of theory<sup>28</sup>, and here the calculations are performed at the G3(MP2,CC)//B3LYP/6-311G\*\* level of theory. Since our goal is to simulate the chemistry at high  $C_2H_2$  concentrations, H-abstraction between closed-shell species and  $C_2H_3$  radical is important as well. In Table 2, the rate parameters are summarized; in Figure 6, the 14 sites that H or  $C_2H_3$  can attack on 1-ETN and 2-ETN are labeled. The H-abstraction rate is relatively insensitive to the attack site; however, the small variations in rates for different sites may cause a change in product distribution. For example, in the case of 2-ETN, ANT formation is only possible when the reaction takes place on site 1 in Figure 6, while PTR formation relies on the reaction taking place on site 7. The corresponding reactions, 2-ETN+H (or  $C_2H_3$ )  $\rightarrow$  N1-CS4+H<sub>2</sub> (or  $C_2H_4$ ) and 2-ETN+H (or  $C_2H_3$ )  $\rightarrow$  N1-CS10+H<sub>2</sub> (or  $C_2H_4$ ), have slightly higher energy barriers which disfavor the formation of ANT and PTR, such that  $C_{14}H_8$  isomers are the preferred final products. The model presented here, based on high-level ab initio quantum calculations, has the ability to accurately predict the distribution of the various  $C_{14}$  products.

**Table 2.** Reaction rate parameters of the H-abstraction reactions calculated in this work in the form of  $AT^n \exp(-E/RT)$ ; the units are  $cm^3 mol^{-1} s^{-1}$  and kcal/mol.

Reaction	A	n	E	Reaction	A	n	E
1-ETN+H $\rightarrow$ N1-CS6+H <sub>2</sub>	3.04e+07	1.99	15.9	1-ETN+C <sub>2</sub> H <sub>3</sub> $\rightarrow$ N1-CS6+C <sub>2</sub> H <sub>4</sub>	2.00e-02	4.18	7.03

1-ETN+H→N1-CS7+H <sub>2</sub>	2.45e+07	2.01	15.8	1-ETN+C <sub>2</sub> H <sub>3</sub> →N1-CS7+C <sub>2</sub> H <sub>4</sub>	2.14e-02	4.21	7.13
1-ETN+H→N1-CS8+H <sub>2</sub>	2.46e+07	2.00	15.8	1-ETN+C <sub>2</sub> H <sub>3</sub> →N1-CS8+C <sub>2</sub> H <sub>4</sub>	1.69e-02	4.18	6.94
1-ETN+H→N1-CS9+H <sub>2</sub>	2.50e+07	1.99	15.0	1-ETN+C <sub>2</sub> H <sub>3</sub> →N1-CS9+C <sub>2</sub> H <sub>4</sub>	1.58e-02	4.18	6.23
1-ETN+H→N1-CS10+H <sub>2</sub>	2.38e+07	2.01	14.8	1-ETN+C <sub>2</sub> H <sub>3</sub> →N1-CS10+C <sub>2</sub> H <sub>4</sub>	1.76e-02	4.22	6.39
1-ETN+H→N1-CS11+H <sub>2</sub>	2.29e+07	2.01	14.7	1-ETN+C <sub>2</sub> H <sub>3</sub> →N1-CS11+C <sub>2</sub> H <sub>4</sub>	1.96e-02	4.23	6.38
1-ETN+H→N1-CS12+H <sub>2</sub>	1.81e+07	2.01	16.1	1-ETN+C <sub>2</sub> H <sub>3</sub> →N1-CS12+C <sub>2</sub> H <sub>4</sub>	2.92e-03	4.27	7.00
2-ETN+H→N1-CS4+H <sub>2</sub>	3.11e+07	1.99	16.7	2-ETN+C <sub>2</sub> H <sub>3</sub> →N1-CS4+C <sub>2</sub> H <sub>4</sub>	2.12e-02	4.16	7.56
2-ETN+H→N1-CS5+H <sub>2</sub>	2.44e+07	2.00	16.0	2-ETN+C <sub>2</sub> H <sub>3</sub> →N1-CS5+C <sub>2</sub> H <sub>4</sub>	1.67e-02	4.18	7.04
2-ETN+H→N1-CS6+H <sub>2</sub>	2.43e+07	2.00	15.3	2-ETN+C <sub>2</sub> H <sub>3</sub> →N1-CS6+C <sub>2</sub> H <sub>4</sub>	1.44e-02	4.19	6.60
2-ETN+H→N1-CS7+H <sub>2</sub>	2.36e+07	2.01	15.3	2-ETN+C <sub>2</sub> H <sub>3</sub> →N1-CS7+C <sub>2</sub> H <sub>4</sub>	1.56e-02	4.23	6.88
2-ETN+H→N1-CS8+H <sub>2</sub>	2.37e+07	2.01	15.2	2-ETN+C <sub>2</sub> H <sub>3</sub> →N1-CS8+C <sub>2</sub> H <sub>4</sub>	1.61e-02	4.23	6.78
2-ETN+H→N1-CS9+H <sub>2</sub>	2.42e+07	2.00	15.5	2-ETN+C <sub>2</sub> H <sub>3</sub> →N1-CS9+C <sub>2</sub> H <sub>4</sub>	1.56e-02	4.19	6.62
2-ETN+H→N1-CS10+H <sub>2</sub>	3.34e+07	1.97	16.3	2-ETN+C <sub>2</sub> H <sub>3</sub> →N1-CS10+C <sub>2</sub> H <sub>4</sub>	1.76e-02	4.13	7.06
ACN+H→N1-CS38+H <sub>2</sub>	5.13e+07	2.00	17.9	ACN+C <sub>2</sub> H <sub>3</sub> →N1-CS38+C <sub>2</sub> H <sub>4</sub>	3.52e-02	4.20	7.70
ACN+H→N1-CS39+H <sub>2</sub>	4.48e+07	2.01	15.8	ACN+C <sub>2</sub> H <sub>3</sub> →N1-CS39+C <sub>2</sub> H <sub>4</sub>	3.72e-02	4.21	7.20
ACN+H→N1-CS40+H <sub>2</sub>	4.11e+07	2.02	17.0	ACN+C <sub>2</sub> H <sub>3</sub> →N1-CS40+C <sub>2</sub> H <sub>4</sub>	2.75e-02	4.24	7.51
ACN+H→N1-CS41+H <sub>2</sub>	1.83e+08	1.89	19.2	ACN+C <sub>2</sub> H <sub>3</sub> →N1-CS41+C <sub>2</sub> H <sub>4</sub>	2.66e-01	4.01	9.45
1-VNP+H→N2-1+H <sub>2</sub>	6.07e+07	1.91	15.3	1-VNP+C <sub>2</sub> H <sub>3</sub> →N2-1+C <sub>2</sub> H <sub>4</sub>	8.64e-04	4.52	6.58
1-VNP+H→N7-1+H <sub>2</sub>	1.47e+06	2.23	14.0	1-VNP+C <sub>2</sub> H <sub>3</sub> →N7-1+C <sub>2</sub> H <sub>4</sub>	6.64e-04	4.49	5.35
1-VNP+H→N11-1+H <sub>2</sub>	2.69e+06	2.18	13.1	1-VNP+C <sub>2</sub> H <sub>3</sub> →N11-1+C <sub>2</sub> H <sub>4</sub>	2.16e-03	4.29	4.66
2-VNP+H→N2-2+H <sub>2</sub>	2.32e+07	2.02	15.2	2-VNP+C <sub>2</sub> H <sub>3</sub> →N2-2+C <sub>2</sub> H <sub>4</sub>	3.16e-03	4.40	6.67
2-VNP+H→N8-2+H <sub>2</sub>	1.52e+07	2.06	13.1	2-VNP+C <sub>2</sub> H <sub>3</sub> →N8-2+C <sub>2</sub> H <sub>4</sub>	6.56e-03	4.22	3.97
2-VNP+H→N11-2+H <sub>2</sub>	9.92e+06	2.09	15.3	2-VNP+C <sub>2</sub> H <sub>3</sub> →N11-2+C <sub>2</sub> H <sub>4</sub>	1.56e-03	4.33	6.30

H-abstraction on ACN is calculated for the first time, which initiates the C<sub>14</sub>H<sub>9</sub> network discussed above. Although N1-CS38 leads to the most stable C<sub>14</sub>H<sub>8</sub> product, the fastest ACN + H or ACN + C<sub>2</sub>H<sub>3</sub> reactions generate N1-CS39 which has the lowest energy barrier. This implies that the most abundant C<sub>14</sub>H<sub>8</sub> isomer could be N2-CS30, instead of N1-CS51, once a significant amount of ACN has accumulated in the reactor. Another important aspect of H-abstraction is related to 1-VNP and 2-VNP. In the Modified Frenklach<sup>22,23</sup> pathway, the second C<sub>2</sub>H<sub>2</sub> is attacked by species with a radical on the aromatic ring (N7-1, N11-1, N8-2, and N11-2) rather than by the direct adduct (N2-1 and N2-2) of the first C<sub>2</sub>H<sub>2</sub> addition. H migration can occur in the Modified Frenklach pathway via unimolecular isomerization from N2-1 and N2-2 to N7-1, N11-1, N8-2, and N11-2, or via two-step H transfer reactions between these isomers. H abstraction from H<sub>2</sub>/C<sub>2</sub>H<sub>4</sub> by N2-1 and N2-2 produces VNP; a second H-abstraction abstracts H/C<sub>2</sub>H<sub>3</sub> on VNP at different sites to generate aryl radical species (1-N7, 1-N11, 2-N8, and 2-N11). The kinetics of VNP H-abstraction are given in Table 2 and illustrated in Figure 6.

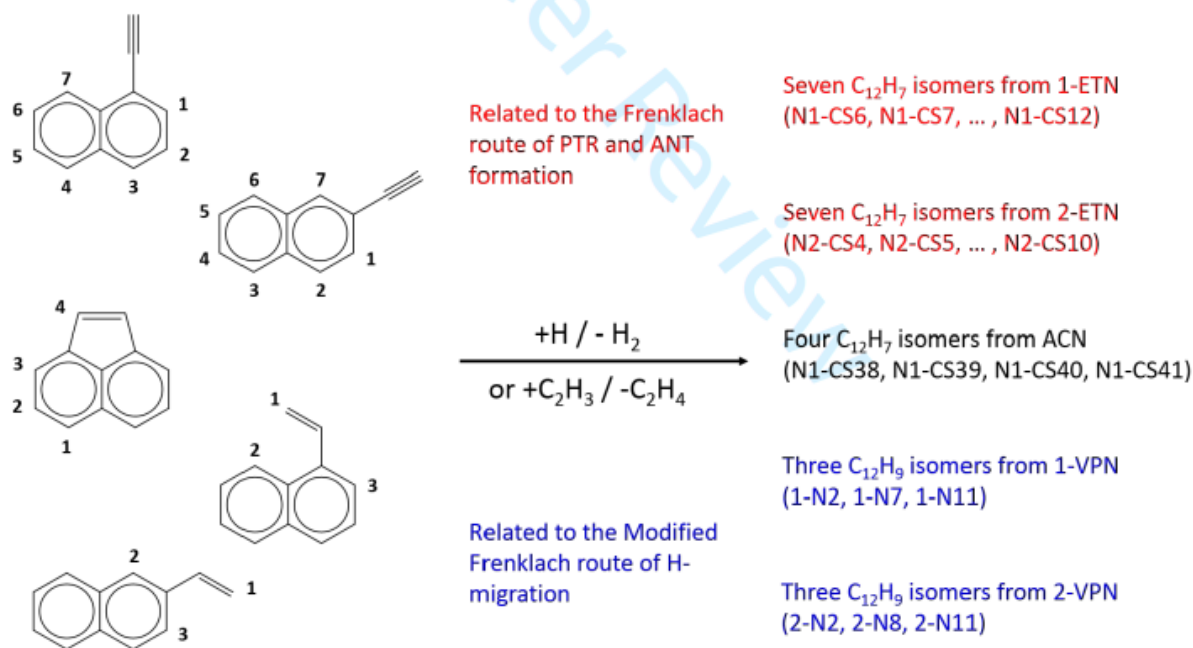


Figure 6. H-abstraction reactions calculated at the G3(MP2,CC)//B3LYP/6-311G\*\* level of theory and included in the naphthalenyl HACA model.

#### Product Formation and Pathway Analysis of 1-Naphthalenyl Radical + Acetylene

Product formation starting from  $1-C_{10}H_7 + C_2H_2$  has been modeled for four conditions: 30 Torr, 800 K; 300 Torr, 800 K; 30 Torr, 1500 K; and 300 Torr, 1500 K. The results are shown in Figure 7. The condition 1500 K/30 Torr is chosen to model high temperature pyrolysis, such as Parker's experiments<sup>32</sup>, while 800 K/30 Torr is an intermediate temperature and represents conditions that can be achieved in the Green group laser absorption spectroscopy/VUV photoionization mass spectrometry apparatus<sup>63</sup>; efforts are currently underway to investigate the naphthalenyl radical HACA reactions experimentally using this apparatus. The initial mole fraction of  $1-C_{10}H_7$  in the simulations is set as 0.01% at 30 Torr (pure  $C_2H_2$ ) and 0.001% at 300 Torr (10%  $C_2H_2 + 90\%$  Helium), because the initial radical concentration through pyrolysis in Parker et al.'s experiments is less than 0.1%. The addition of helium was used to increase the pressure while maintaining the same absolute concentration for both  $1-C_{10}H_7$  and  $C_2H_2$  to control the reactivity. At 800 K, the 0.01% (30 Torr) and 0.001% (300 Torr) radical concentration correspond to  $3.6 \times 10^{13}$  molecule/cm<sup>3</sup>, which is in the range of the radical concentration that can be generated in the Green group flash photolysis apparatus. Based on Guan et al.'s study<sup>64</sup>, the micro-reactor system used in Parker et al.'s pyrolysis experiments<sup>32</sup> has the residence time ranging from 0.025 to 0.150 ms, so we plot the results on that timescale in Figure 7.

At 800 K, the model predicts that the dominant products of  $1-C_{10}H_7 + C_2H_2$  arise from the first  $C_2H_2$  addition, while chemistry involving subsequent  $C_2H_2$  additions is negligible. ACN is the most stable among the bimolecular products, and 1-N8 has the lowest energy on the  $C_{12}H_9$  PES due to its resonance stabilized structure and two aromatic rings. At 800 K and 30 Torr, ACN is immediately formed within a short time as the most abundant product; on the other hand, 1-N8 is predicted to

be the abundant product at 300 Torr. The competition between unimolecular adducts and bimolecular products as a result of the change in pressure can be seen in Figure 7. Both 1-N8 and AN1 adducts become more abundant relative to ACN (+ H) at 300 Torr in Figure 7(b). The high barrier ( $> 40$  kcal/mol) from 1-N8 to ACN + H slows down ACN formation and contributes to the long lifetime of 1-N8 at 800 K. Here we only present reaction time up to 0.10 ms at 800 K and 300 Torr; however, longer reaction times have been modeled and the conversion from 1-N8 to ACN + H happens on a time scale of about 0.50 ms, as seen in the Supporting Information.

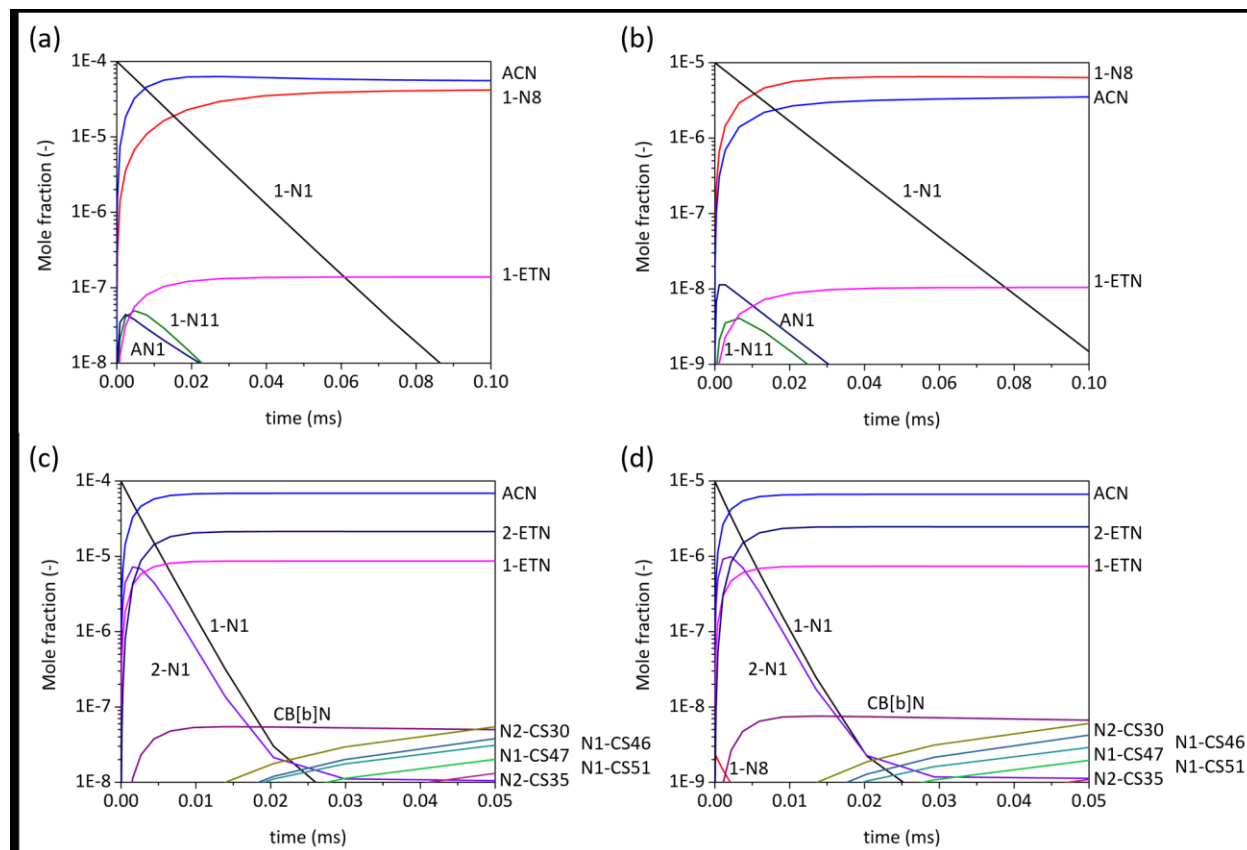


**Figure 7. Simulated species concentration profiles starting from  $1\text{-C}_{10}\text{H}_7 + \text{C}_2\text{H}_2$ . (a) 30 Torr, 800 K, (b) 300 Torr, 800 K, (c) 30 Torr, 1500 K, (d) 300 Torr, 1500 K.**

At 1500 K, ACN is predicted as the leading product at both 30 Torr and 300 Torr, shown in Figure 7(c) and (d). Due to the activation from high temperatures, the concentration decay of 1-N8 as it converts to ACN happens within a short time scale, such that 1-N8 can only be observed with perceptible amount at the higher pressure of 300 Torr within  $5\text{e-}3$  ms in Figure 7(d). At higher temperatures like 1500 K, after reactants are activated, multiple isomerization and dissociation reactions become competitive with one another and with collisional stabilization.<sup>47</sup> The formation of 2-N1 ( $2\text{-C}_{10}\text{H}_7$ ) and 2-ETN indicates that reactions in the  $2\text{-C}_{10}\text{H}_7$  network on the overall  $\text{C}_{12}\text{H}_9$  PES are involved. Moreover, five  $\text{C}_{14}\text{H}_8$  isomers – N2-CS30, N1-CS46, N1-CS47, N1-CS51, and N2-CS35 – appear as the second most abundant group of isomers after  $\text{C}_{12}\text{H}_8$  products. The lumped concentration of these species in our simulations is about an order of magnitude higher than PTR +

ANT. This observation is consistent with Parker's experiments<sup>32</sup> where signals of C<sub>14</sub>H<sub>8</sub> isomers were measured, but not C<sub>14</sub>H<sub>10</sub> species.

A detailed reaction pathway analysis of 1-C<sub>10</sub>H<sub>7</sub>+C<sub>2</sub>H<sub>2</sub> at 1500 K is given in Figure 8; the ROP analysis was performed at an early time (1e-6 sec), and the values presented are the percentages of reactants converted into products. At 1500 K and 30 Torr, 66% of 1-C<sub>10</sub>H<sub>7</sub> directly reacts into ACN + H, and 8.5% into 1-ETN + H. The fraction drops to 56% and 7.1% as the pressure increases to 300 Torr, because the direct pathways to bimolecular products are pressure-dependent and less favored at high pressure. In contrast, the formation of 1-N2 and 1-N8 adducts accounts for more than five times more 1-C<sub>10</sub>H<sub>7</sub> consumption at 300 Torr than at 30 Torr. On the C<sub>10</sub>H<sub>7</sub> PES, there are two routes converting 1-C<sub>10</sub>H<sub>7</sub> into 2-C<sub>10</sub>H<sub>7</sub>: 1-C<sub>10</sub>H<sub>7</sub>(+M)→2-C<sub>10</sub>H<sub>7</sub>(+M) [major] and 1-C<sub>10</sub>H<sub>7</sub>(+M)→1-methylenyl-1H-indene (C<sub>10</sub>H<sub>7</sub>-3) →2-C<sub>10</sub>H<sub>7</sub>(+M) [minor]. According to Mebel et al.'s calculations<sup>55</sup>, the barrier to isomerization between 1-C<sub>10</sub>H<sub>7</sub> and 2-C<sub>10</sub>H<sub>7</sub> is 60 kcal/mol. With the activation from high temperatures, the direct isomerization overcomes this high barrier to consume 21% and 26% of 1-C<sub>10</sub>H<sub>7</sub> at 30 Torr and 300 Torr respectively. Once 2-C<sub>10</sub>H<sub>7</sub> is generated, it diverges into several pathways, but ends up with the same product, 2-ETN, which is the second most abundant product at 1500 K.

Relatively little is known about further reactions after ACN formation in naphthalenyl radical HACA chemistry. By implementing H-abstraction reactions from ab-initio calculations and C-H bond dissociation reactions in the current model, we have found that ACN reacts to produce four C<sub>12</sub>H<sub>7</sub> radicals: N1-CS38, N1-CS39, N1-CS40, and N1-CS41. The most important pathway is H-abstraction involving H atom, which is not pressure dependent. Therefore, Figure 8 shows that the ROP of these four radicals have no difference as pressure varies. The radicals then react with the second C<sub>2</sub>H<sub>2</sub> via formally direct pathways to generate C<sub>14</sub>H<sub>8</sub> isomers. All the C<sub>14</sub>H<sub>8</sub> isomers in Figure 8 have 6,6,5-member ring structure like ACN, so they have stable thermochemical properties. As shown in the PES in Figure 4, N1-CS51 (pyracyclene) is the most stable C<sub>14</sub>H<sub>8</sub> isomer, and its formation surpasses the formation of N2-CS35 from N1-CS38. N2-CS30 formed from N1-CS39 has the highest concentration in our simulation, since the H-abstraction from ACN into N1-CS39 is the fastest and contributes large flux from ACN to N2-CS30.

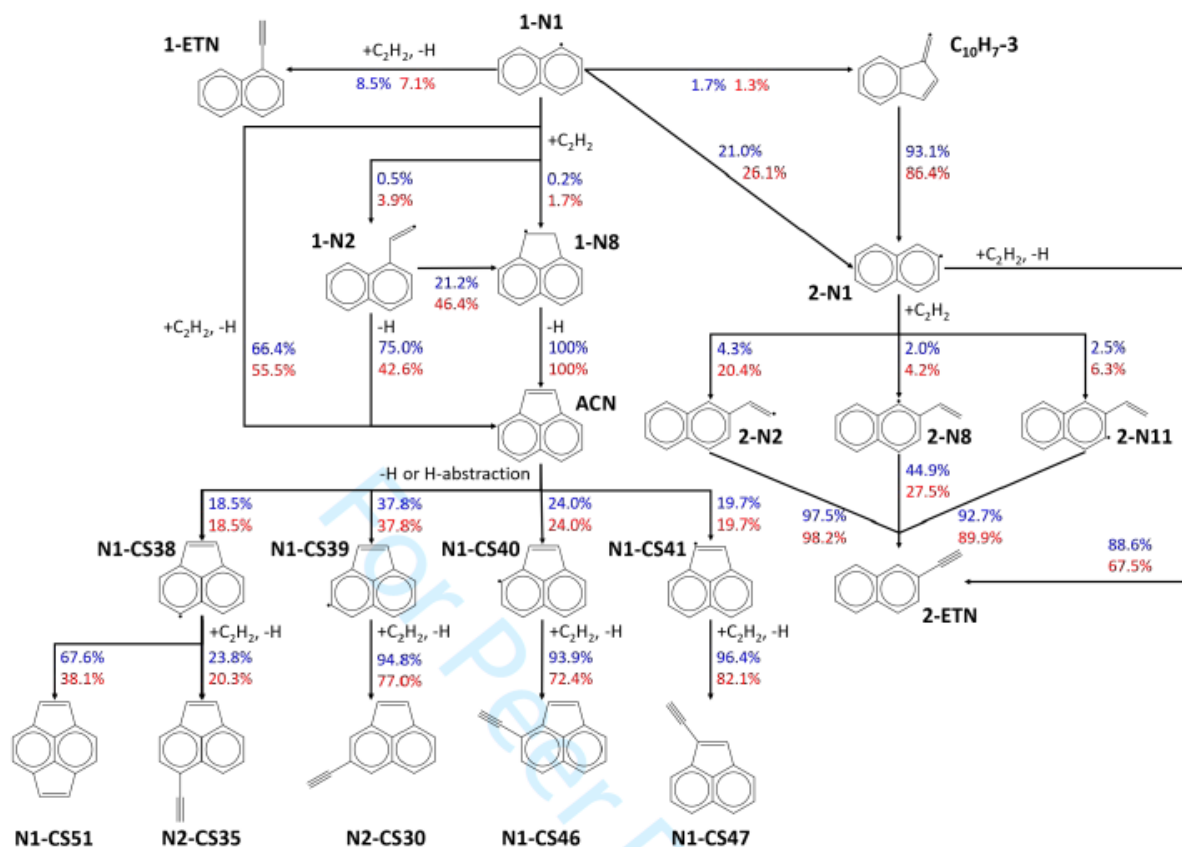


Figure 8. Important pathways and ROP analysis of 1-C<sub>10</sub>H<sub>7</sub> + C<sub>2</sub>H<sub>2</sub> at 1500 K. ROP values are the percentages of reactants converted into products, and evaluated at  $t = 1e-6$  sec. The values in blue are for 30 Torr, and red for 300 Torr.

### Product Formation and Pathway Analysis of 2-Naphthalenyl Radical + Acetylene

The reaction of 2-C<sub>10</sub>H<sub>7</sub> + C<sub>2</sub>H<sub>2</sub> was simulated with the same initial composition as the case of 1-C<sub>10</sub>H<sub>7</sub> + C<sub>2</sub>H<sub>2</sub> at four  $T, P$  conditions. In Figure 9, time profiles of 2-C<sub>10</sub>H<sub>7</sub> and a variety of products are given up to 0.10 ms to observe the appearance of products of second C<sub>2</sub>H<sub>2</sub> addition at 1500 K. At 800 K, the rise of adducts including 2-N2 (direct adduct), 2-N8, and 2-N11 appears within 0.010 ms, and starts to decrease after some time. Unlike the 1-C<sub>10</sub>H<sub>7</sub> + C<sub>2</sub>H<sub>2</sub> reaction which was dominated by the formation of ACN + H, reactions involving a second C<sub>2</sub>H<sub>2</sub> addition to the adducts from the first C<sub>2</sub>H<sub>2</sub> addition are favored to generate PTR and ANT. After 0.05 ms in the model prediction, both PTR and ANT with three fused benzene rings have the highest concentration compared to other products. This behavior is different from Parker et al.'s experiments, where no PTR and ANT signals were observed from room temperature to 1500 K.<sup>32</sup> In Parker et al.'s work<sup>32</sup>, the mass spectrum of products of the 2-naphthylenyl + C<sub>2</sub>H<sub>2</sub> at 1000 K was measured, and at  $m/z$  178 no peak clearly above the noise was noticed. One possible reason is the small radical concentration due to slow dissociation of idonaphthalene at  $T \leq 1000$  K. Lifshitz et al. estimated the dissociation rate constant to be  $4.84 \text{ s}^{-1}$  at 1000 K, so at that temperature only a tiny amount of naphthylenyl radicals would be generated within the very short (<0.15 ms) residence time in Parker et al.'s experiments. With the small radical concentration in the reactor, the total product formation rate and so yield was reduced,

and also the product distribution shifted, because some reaction pathways (e.g. the Frenklach pathways from naphthalene to  $C_{14}H_{10}$ ) involve more than one radical.

However, the prediction of abundant PTR and ANT is consistent with our preliminary measurements<sup>65</sup> using a flash photolysis/time-of-flight mass spectrometry (TOF-MS) apparatus<sup>63</sup> from 600 K to 800 K and 10 to 25 Torr measuring the product formation of  $2-C_{10}H_7 + C_2H_2$ . The radical concentration is expected to be much higher in the flash photolysis experiments compared to the pyrolysis experiments under 1000 K. Clear peaks with time-dependence at  $m/z$  178 belonging to PTR and ANT are seen in the mass spectra within several ms; a detailed comparison between the current model predictions and direct measurements at 800 K and other intermediate temperatures will be reported in an upcoming publication.

Three newly calculated  $C_{12}H_9$  isomers in this work, 2-N14, 2-N16, and 2-N17, have longer lifetimes than other radical species. They are not easily accessible through the surrounding high energy transition states, but that makes these deep wells less reactive as well. They start from negligible concentration, and accumulate to the same level as 2-N2, 2-N8, and 2-N11 at  $t = 100$  us. The resonance-stabilized structures are responsible for their stability: 2-N14 is a benzylic radical, while 2-N16 and 2-N17 have radical centers on a four-member ring stabilized by two aromatic rings. In Figure 3, ACNV2+H are the third most stable bimolecular product channel after PTR+H and ANT+H. Although we cannot see ACNV2 in Figure 9(a) and Figure 9(b), it is predicted to be formed about 1-2% as much as PTR or ANT. According to our calculations, ACNV2 is mainly produced by the well-skipping reaction of  $2-N8 + C_2H_2 \rightarrow ACNV2 + H$ .

When the temperature is increased to 1500 K, 2-ETN becomes the most abundant product followed by ACN, and the combined concentration of PTR and ANT is lower than the concentration of 2-ETN by more than three orders of magnitude. Therefore, PTR and ANT are not shown in Figure 9. Again, this product distribution is in qualitative agreement with Parker et al.'s experiments<sup>32</sup> in which only  $m/z$  152 signals were observed in the pyrolysis reactor at high temperatures, and no  $m/z$  178 peaks were found due to the negligible amount of PTR and ANT. As in the case of  $1-C_{10}H_7 + C_2H_2$ , the  $2-C_{10}H_7 + C_2H_2$  reaction is more likely to stay on the  $C_{12}H_9$  PES and finally dissociate into bimolecular products instead of reacting with a second  $C_2H_2$  at high temperatures. 2-ETN is formed by the direct well skipping pathways or two-step routes with adducts 2-N2, 2-N8, or 2-N11 as intermediates, shown in Figure 10. The pressure increase from 30 Torr to 300 Torr decreases the consumption of  $2-C_{10}H_7$  by the direct well skipping pathway from 76.7% to 54.3%. H-abstraction and dissociation reactions involving 2-ETN potentially can produce PTR and ANT radicals on the  $C_{14}H_9$  PES as reported by Liu et al.<sup>28</sup>. This is the Frenklach pathway, important in phenyl radical HACA chemistry for naphthalene formation. However, in the case of  $2-C_{10}H_7$ , only two out of seven H-atom sites lead to formation of the additional aromatic ring. The remaining five sites can undergo H-abstraction or dissociation reactions, but further  $C_2H_2$  addition will not form an extra six-member ring. In Figure 10 ROP analysis, the pathways related to ANT and PTR only compose 22.7% at 1500 K, 30 Torr (23.6% at 1500 K, 300 Torr) of the 2-ETN consumption, which results in less ANT and PTR formation than naphthalene formation in the analogous case of phenyl radical +  $C_2H_2$  at combustion-like temperatures.

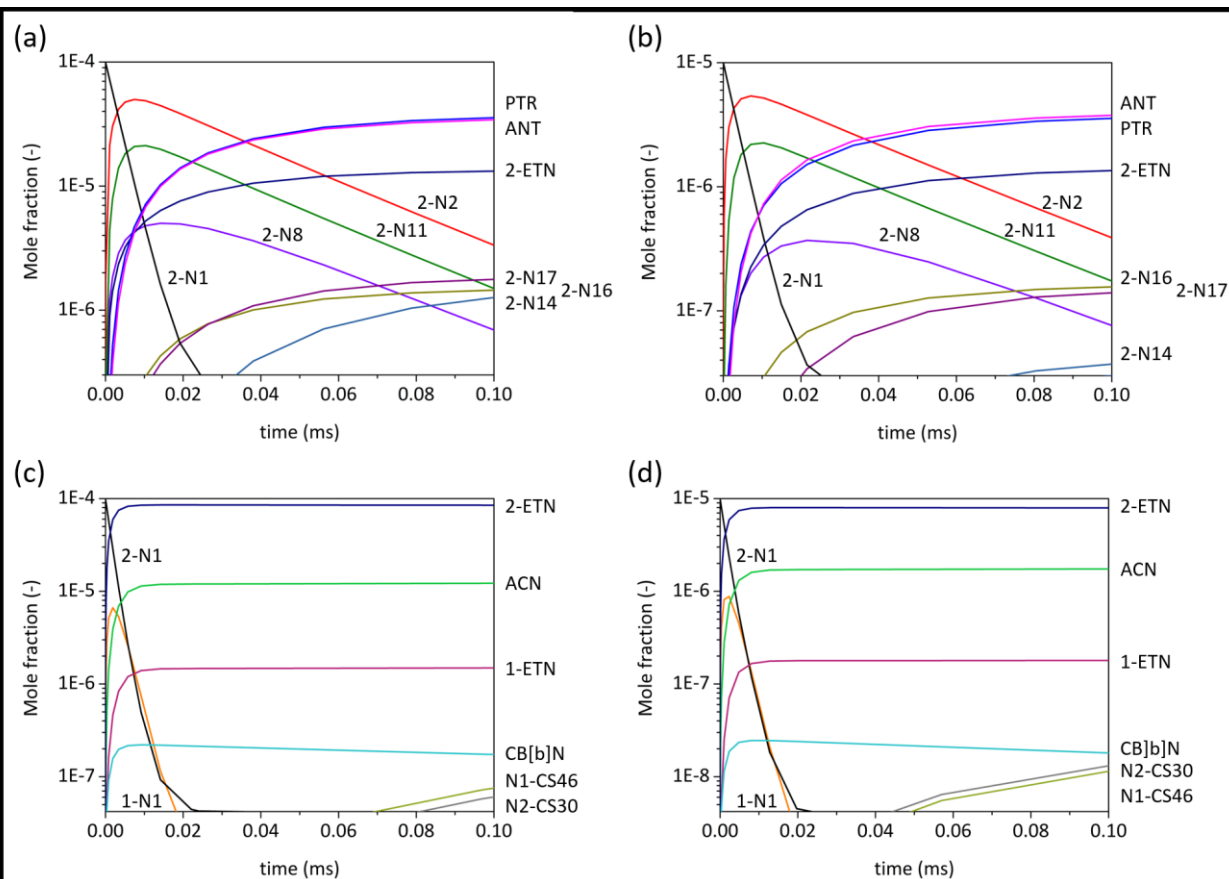


Figure 9. Simulated species concentration profiles starting from  $2\text{-C}_{10}\text{H}_7 + \text{C}_2\text{H}_2$ . (a) 30 Torr, 800 K, (b) 300 Torr, 800 K, (c) 30 Torr, 1200 K, (d) 300 Torr, 1200 K.

The formation of ACN from  $2\text{-C}_{10}\text{H}_7 + \text{C}_2\text{H}_2$  was experimentally measured by Parker et al.<sup>26</sup>, but there were no previous kinetic models supporting the measurement. Here we use the comprehensive model to discover three pathways. First, the isomerization from  $2\text{-C}_{10}\text{H}_7$  to  $1\text{-C}_{10}\text{H}_7$  (including the route with the intermediate  $\text{C}_{10}\text{H}_7\text{-3}$ ) followed by the formally direct pathway of  $1\text{-C}_{10}\text{H}_7 + \text{C}_2\text{H}_2$ . Second, a direct formally direct pathway from  $2\text{-C}_{10}\text{H}_7 + \text{C}_2\text{H}_2$  to ACN + H. Third, 2-N8 is generated from  $2\text{-C}_{10}\text{H}_7 + \text{C}_2\text{H}_2$ , then isomerizes to 1-N11 which can directly form ACN + H. The first pathway is preferred at high pressures, because the isomerization from  $2\text{-C}_{10}\text{H}_7$  to  $1\text{-C}_{10}\text{H}_7$  is the critical step, and the fraction of  $2\text{-C}_{10}\text{H}_7$  consumption via isomerization to  $1\text{-C}_{10}\text{H}_7$  increases from 12% at 30 Torr to 18% at 300 Torr. After  $1\text{-C}_{10}\text{H}_7$  appears in the model, several pathways become available though most of them end up with ACN + H. The second pathway is represented by the second reaction in Table 1. Although this formally direct pathway across the overall  $\text{C}_{12}\text{H}_9$  PES exhibits faster kinetics at low pressures, it is a minor channel accounting for less than 1% the  $2\text{-C}_{10}\text{H}_7$  consumption at 1500 K and 30 Torr. The third route has three steps -  $2\text{-C}_{10}\text{H}_7 + \text{C}_2\text{H}_2(+\text{M}) \rightarrow 2\text{-N8}(+\text{M})$ ,  $2\text{-N8}(+\text{M}) \rightarrow 1\text{-N11}(+\text{M})$ , and  $1\text{-N11}(+\text{M}) \rightarrow \text{ACN} + \text{H}(+\text{M})$  - and the first two steps favor high pressure conditions. Similar to the first pathway, once  $\text{C}_{12}\text{H}_9$  isomers such as 1-N11 on the  $1\text{-C}_{10}\text{H}_7 + \text{C}_2\text{H}_2$  network are formed, ACN is expected to be the final product. Therefore, an increase in ACN abundance is shown in Figure 9 as pressure increases at 1500 K.

$C_{14}H_8$  formation was also observed in the  $2-C_{10}H_7 + C_2H_2$  experiment by Parker et al.<sup>26</sup> As seen in Figure 9, two  $C_{14}H_8$  isomers N1-CS46 and N2-CS30 are predicted by our model to form in noticeable amounts, more than other  $C_{14}H_8$  or  $C_{14}H_{10}$  species. Despite the consistency with Parker et al.'s experiment, the pathway of their formation is surprising. The secondary reaction of ACN in Figure 10, instead of the major product 2-ETN, results in the  $C_{14}H_8$  products. In comparison, Kislov et al. predict all  $C_{14}H_8$  products are derived from 2-ETN<sup>34</sup>. Future experiments that can distinguish isomers will be helpful to validate the prediction in this work.

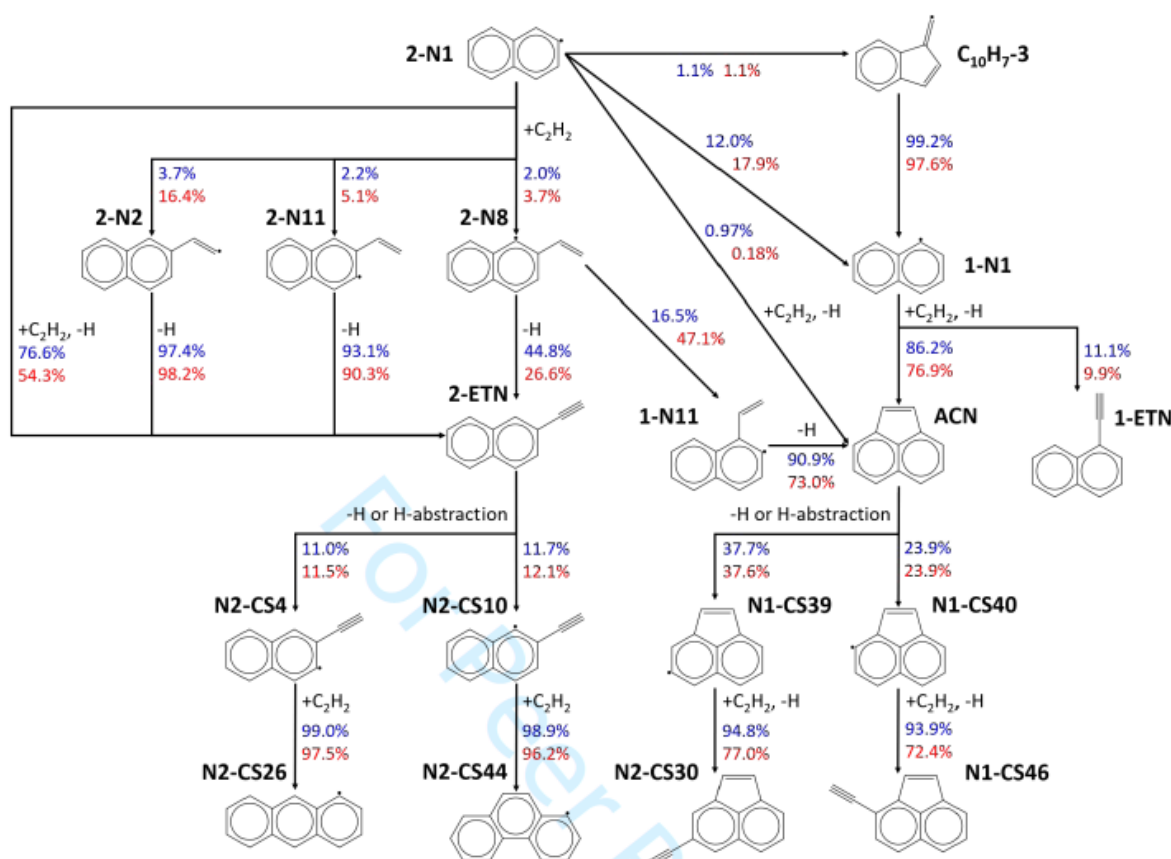


Figure 10. Important pathways and ROP analysis of  $2-C_{10}H_7 + C_2H_2$  at 1500 K. ROP values are the percentages of reactants converted into products, and evaluated at  $t = 1e-6$  sec. The values in blue are for 30 Torr, and red for 300 Torr

## Conclusions

A pressure-dependent model describing naphthalenyl radical (1-C<sub>10</sub>H<sub>7</sub> and 2-C<sub>10</sub>H<sub>7</sub>) HACA chemistry has been developed including C<sub>12</sub>H<sub>9</sub>, C<sub>14</sub>H<sub>9</sub>, and C<sub>14</sub>H<sub>11</sub> PESs as well as other reactions important over a wide range of  $T$ ,  $P$  conditions considered in this work. Numerous new species and transition states have been calculated to explain the unexpected results of Parker et al.'s experiments<sup>32</sup> at combustion-like temperatures. In the previous experiments, ACN was measured starting from 2-C<sub>10</sub>H<sub>7</sub> + C<sub>2</sub>H<sub>2</sub>, but the reaction pathways responsible for its formation were unclear. Here, a new bridge species, N-shared, was found to connect two entry points on the overall C<sub>12</sub>H<sub>9</sub> PES, and reaction pathways on a validated C<sub>10</sub>H<sub>7</sub> PES based on ab-initio calculations are shown to enable ACN formation. At high temperatures, formally direct reactions such as 2-C<sub>10</sub>H<sub>7</sub>(+M) → 1-C<sub>10</sub>H<sub>7</sub>(+M) and 2-C<sub>10</sub>H<sub>7</sub> + C<sub>2</sub>H<sub>2</sub>(+M) → ACN + H(+M) exhibit pressure-dependent kinetics and play an important role in formation of the stable bimolecular products, ACN + H.

In Parker et al.'s experiments, at the highest temperatures perceptible C<sub>14</sub>H<sub>8</sub> signals were measured, but no C<sub>14</sub>H<sub>10</sub> signals corresponding to PTR and ANT were observed either from 2-C<sub>10</sub>H<sub>7</sub> + C<sub>2</sub>H<sub>2</sub> or 1-C<sub>10</sub>H<sub>7</sub> + C<sub>2</sub>H<sub>2</sub>. At lower temperatures (e.g. 1000 K) both 2-C<sub>10</sub>H<sub>7</sub> + C<sub>2</sub>H<sub>2</sub> or 1-C<sub>10</sub>H<sub>7</sub> + C<sub>2</sub>H<sub>2</sub> were measured to yield mostly C<sub>12</sub>H<sub>8</sub> products, with only a very weak peak close to the noise level at the mass of C<sub>14</sub>H<sub>10</sub> and even less C<sub>14</sub>H<sub>8</sub> signal.

In the present work we have created a more comprehensive high-accuracy model for this chemistry. The pressure-dependent network on the C<sub>14</sub>H<sub>9</sub> PES has been extended by combining the calculations of Liu et al.<sup>28</sup> with new calculations. Moreover, H-abstraction reactions have been calculated and implemented in the model to connect multiple PESs and improve the accuracy of predicted product distributions. The model-predicted concentration of C<sub>14</sub>H<sub>8</sub> isomers starting from both 1-C<sub>10</sub>H<sub>7</sub> + C<sub>2</sub>H<sub>2</sub> and 2-C<sub>10</sub>H<sub>7</sub> + C<sub>2</sub>H<sub>2</sub> at high temperatures dominates over the concentration of PTR and ANT, which is consistent with Parker et al.'s experimental measurement. The previous experimental work by Parker et al. did not detect significant PTR and ANT production in the temperature range between room temperature and 1500 K. However, it is important to keep in mind that the experiments of Parker et al. at low and intermediate temperatures had very low radical concentrations because the thermal radical formation is much lower at low temperatures. Because the radical concentration is so small in their low temperature experiments, the total product formation rate and so yield is reduced, and also the product distribution shifts, because some reaction pathways (e.g. the Frenklach pathways from naphthalene to C<sub>14</sub>H<sub>10</sub>) involve more than one radical. The present calculations predict which fraction of the radicals go to different products at different conditions, and our calculations predict that around 800 K a significant fraction of the 2-C<sub>10</sub>H<sub>7</sub> radical will go to the three-fused-benzene-ring species PTR and ANT if the radical concentration is in the range of our model. Our interpretation is that the Frenklach HACA pathway to PTR and ANT does actually run at 800 K in systems with high enough radical concentrations, but those products were not detected in the low temperature Parker et al. experiments because the radical concentration was so small at their conditions. Unlike the Parker et al. experiments, our preliminary experiments detected products at  $m/z$  178.<sup>65</sup> We are doing further experimental work in our lab using flash photolysis to generate higher radical concentrations to test this prediction of our model; those experimental results will be reported separately.

## Acknowledgments

We gratefully acknowledge helpful discussions with Prof. Alexander Mebel. This research was supported by SABIC. Te-Chun Chu received additional fellowship funding from the Think Global Education Trust (Taiwan).

## Conflict of Interest Statement

The authors declare no competing financial interest.

## Supporting Information Available

Supporting information with simulation of  $1\text{-C}_{10}\text{H}_7 + \text{C}_2\text{H}_2$ , 300 Torr, 800 K up to 1.0 ms

Optimized geometry of all species and transition states

Arkane input files including molecular information

Chemkin mechanism (kinetics + thermochemistry), species transport properties, and species dictionary

## Author Information

### Corresponding Author

William H. Green, E-mail: [whgreen@mit.edu](mailto:whgreen@mit.edu)

### ORCID:

Te-Chun Chu 0000-0002-8475-7697

Mica C. Smith 0000-0003-4534-7246

Jeehyun Yang 0000-0002-1551-2610

Mengjie Liu 0000-0003-2414-1986

William H. Green 0000-0003-2603-9694

## References

1. Li, C. e.; Kuan, B.; Lee, W. J.; Burke, N.; Patel, J. The non-catalytic partial oxidation of methane in a flow tube reactor using indirect induction heating – An experimental and kinetic modelling study. *Chemical Engineering Science* 2018, 187, 189-199.
2. Köhler, M.; Oßwald, P.; Xu, H.; Kathrotia, T.; Hasse, C.; Riedel, U. Speciation data for fuel-rich methane oxy-combustion and reforming under prototypical partial oxidation conditions. *Chemical Engineering Science* 2016, 139, 249-260.
3. Skjøth-Rasmussen, M. S.; Glarborg, P.; Østberg, M.; Johannessen, J. T.; Livbjerg, H.; Jensen, A. D.; Christensen, T. S. Formation of polycyclic aromatic hydrocarbons and soot in fuel-rich oxidation of methane in a laminar flow reactor. *Combustion and Flame* 2004, 136, 91-128.
4. Chu, T.-C.; Buras, Z. J.; Oßwald, P.; Liu, M.; Goldman, M. J.; Green, W. H. Modeling of aromatics formation in fuel-rich methane oxy-combustion with an automatically generated pressure-dependent mechanism. *Physical Chemistry Chemical Physics* 2019, 21, 813-832.
5. Yan, F.; Xu, L.; Wang, Y.; Park, S.; Sarathy, S. M.; Chung, S. H. On the opposing effects of methanol and ethanol addition on PAH and soot formation in ethylene counterflow diffusion flames. *Combustion and Flame* 2019, 202, 228-242.
6. Slavinskaya, N. A.; Riedel, U.; Dworkin, S. B.; Thomson, M. J. Detailed numerical modeling of PAH formation and growth in non-premixed ethylene and ethane flames. *Combustion and Flame* 2012, 159, 979-995.
7. Wang, H.; Frenklach, M. A detailed kinetic modeling study of aromatics formation in laminar premixed acetylene and ethylene flames. *Combustion and Flame* 1997, 110, 173-221.
8. Yang, J.; Zhao, L.; Yuan, W.; Qi, F.; Li, Y. Experimental and kinetic modeling investigation on laminar premixed benzene flames with various equivalence ratios. *Proceedings of the Combustion Institute* 2015, 35, 855-862.
9. Yang, B.; Li, Y.; Wei, L.; Huang, C.; Wang, J.; Tian, Z.; Yang, R.; Sheng, L.; Zhang, Y.; Qi, F. An experimental study of the premixed benzene/oxygen/argon flame with tunable synchrotron photoionization. *Proceedings of the Combustion Institute* 2007, 31, 555-563.
10. Defoeux, F.; Dias, V.; Renard, C.; Van Tiggelen, P. J.; Vandooren, J. Experimental investigation of the structure of a sooting premixed benzene/oxygen/argon flame burning at low pressure. *Proceedings of the Combustion Institute* 2005, 30, 1407-1415.
11. Bittner, J. D.; Howard, J. B. Composition profiles and reaction mechanisms in a near-sooting premixed benzene/oxygen/argon flame. *Symposium (International) on Combustion* 1981, 18, 1105-1116.
12. Johansson, K. O.; Head-Gordon, M. P.; Schrader, P. E.; Wilson, K. R.; Michelsen, H. A. Resonance-stabilized hydrocarbon-radical chain reactions may explain soot inception and growth. *Science* 2018, 361, 997-1000.
13. Wornat, M. J.; Ledesma, E. B.; Sandrowitz, A. K.; Roth, M. J.; Dawsey, S. M.; Qiao, Y.-L.; Chen, W. Polycyclic Aromatic Hydrocarbons Identified in Soot Extracts from Domestic Coal-Burning Stoves of Henan Province, China. *Environmental Science & Technology* 2001, 35, 1943-1952.
14. Finlayson-Pitts, B. J.; Pitts, J. N. Tropospheric Air Pollution: Ozone, Airborne Toxics, Polycyclic Aromatic Hydrocarbons, and Particles. *Science* 1997, 276, 1045-1051.
15. Kholghy, M. R.; Veshkini, A.; Thomson, M. J. The core-shell internal nanostructure of soot – A criterion to model soot maturity. *Carbon* 2016, 100, 508-536.
16. Boström, C.-E.; Gerde, P.; Hanberg, A.; Jernström, B.; Johansson, C.; Kyrklund, T.; Rannug, A.; Törnqvist, M.; Victorin, K.; Westerholm, R. Cancer risk assessment, indicators, and guidelines for polycyclic aromatic hydrocarbons in the ambient air. *Environmental health perspectives* 2002, 110 Suppl 3, 451-488.
17. Shindell, D.; Kuylensstierna, J. C. I.; Vignati, E.; van Dingenen, R.; Amann, M.; Klimont, Z.; Anenberg, S. C.; Müller, N.; Janssens-Maenhout, G.; Raes, F.; Schwartz, J.; Faluvegi, G.; Pozzoli, L.; Kupiainen, K.; Höglund-Isaksson, L.; Emberson, L.; Streets, D.; Ramanathan, V.; Hicks, K.; Oanh, N. T.

- K.; Milly, G.; Williams, M.; Demkine, V.; Fowler, D. Simultaneously Mitigating Near-Term Climate Change and Improving Human Health and Food Security. *Science* 2012, 335, 183-189.
18. McEnally, C. S.; Pfefferle, L. D.; Atakan, B.; Kohse-Höinghaus, K. Studies of aromatic hydrocarbon formation mechanisms in flames: Progress towards closing the fuel gap. *Progress in Energy and Combustion Science* 2006, 32, 247-294.
19. Frenklach, M.; Wang, H. Detailed modeling of soot particle nucleation and growth. *Symposium (International) on Combustion* 1991, 23, 1559-1566.
20. Frenklach, M.; Clary, D. W.; Gardiner, W. C.; Stein, S. E. Detailed kinetic modeling of soot formation in shock-tube pyrolysis of acetylene. *Symposium (International) on Combustion* 1985, 20, 887-901.
21. Wang, H.; Frenklach, M. Calculations of Rate Coefficients for the Chemically Activated Reactions of Acetylene with Vinylic and Aromatic Radicals. *The Journal of Physical Chemistry* 1994, 98, 11465-11489.
22. Moriarty, N. W.; Brown, N. J.; Frenklach, M. Hydrogen Migration in the Phenylethen-2-yl Radical. *The Journal of Physical Chemistry A* 1999, 103, 7127-7135.
23. Frenklach, M.; Moriarty, N. W.; Brown, N. J. Hydrogen migration in polyaromatic growth. *Symposium (International) on Combustion* 1998, 27, 1655-1661.
24. Chu, T.-C.; Buras, Z. J.; Smith, M. C.; Uwagwu, A. B.; Green, W. H. From benzene to naphthalene: direct measurement of reactions and intermediates of phenyl radicals and acetylene. *Physical Chemistry Chemical Physics* 2019, 21, 22248-22258.
25. Yang, T.; Troy, T. P.; Xu, B.; Kostko, O.; Ahmed, M.; Mebel, A. M.; Kaiser, R. I. Hydrogen-Abstraction/Acetylene-Addition Exposed. *Angewandte Chemie International Edition* 2016, 55, 14983-14987.
26. Parker, D. S. N.; Kaiser, R. I.; Troy, T. P.; Ahmed, M. Hydrogen Abstraction/Acetylene Addition Revealed. *Angewandte Chemie International Edition* 2014, 53, 7740-7744.
27. Yu, T.; Lin, M. C. Kinetics of phenyl radical reactions studied by the cavity-ring-down method. *Journal of the American Chemical Society* 1993, 115, 4371-4372.
28. Liu, P.; Li, Z.; Bennett, A.; Lin, H.; Sarathy, S. M.; Roberts, W. L. The site effect on PAHs formation in HACA-based mass growth process. *Combustion and Flame* 2019, 199, 54-68.
29. Mebel, A. M.; Georgievskii, Y.; Jasper, A. W.; Klippenstein, S. J. Temperature- and pressure-dependent rate coefficients for the HACA pathways from benzene to naphthalene. *Proceedings of the Combustion Institute* 2017, 36, 919-926.
30. Tokmakov, I. V.; Lin, M. C. Reaction of Phenyl Radicals with Acetylene: Quantum Chemical Investigation of the Mechanism and Master Equation Analysis of the Kinetics. *Journal of the American Chemical Society* 2003, 125, 11397-11408.
31. Richter, H.; Mazyar, O. A.; Sumathi, R.; Green, W. H.; Howard, J. B.; Bozzelli, J. W. Detailed Kinetic Study of the Growth of Small Polycyclic Aromatic Hydrocarbons. 1. 1-Naphthyl + Ethyne<sup>†</sup>. *The Journal of Physical Chemistry A* 2001, 105, 1561-1573.
32. Parker, D. S. N.; Kaiser, R. I.; Bandyopadhyay, B.; Kostko, O.; Troy, T. P.; Ahmed, M. Unexpected Chemistry from the Reaction of Naphthyl and Acetylene at Combustion-Like Temperatures. *Angewandte Chemie International Edition* 2015, 54, 5421-5424.
33. Frenklach, M.; Singh, R. I.; Mebel, A. M. On the low-temperature limit of HACA. *Proceedings of the Combustion Institute* 2019, 37, 969-976.
34. Kislov, V. V.; Sadovnikov, A. I.; Mebel, A. M. Formation Mechanism of Polycyclic Aromatic Hydrocarbons beyond the Second Aromatic Ring. *The Journal of Physical Chemistry A* 2013, 117, 4794-4816.
35. Frisch, M. J.; Trucks, G. W.; Schlegel, H. B.; Scuseria, G. E.; Robb, M. A.; Cheeseman, J. R.; Scalmani, G.; Barone, V.; Petersson, G. A.; Nakatsuji, H.; Li, X.; Caricato, M.; Marenich, A. V.; Bloino, J.; Janesko, B. G.; Gomperts, R.; Mennucci, B.; Hratchian, H. P.; Ortiz, J. V.; Izmaylov, A. F.; Sonnenberg, J. L.; Williams-Young, D.; Ding, F.; Lipparini, F.; Egidi, F.; Goings, J.; Peng, B.; Petrone, A.;

- Henderson, T.; Ranasinghe, D.; Zakrzewski, V. G.; Gao, J.; Rega, N.; Zheng, G.; Liang, W.; Hada, M.; Ehara, M.; Toyota, K.; Fukuda, R.; Hasegawa, J.; Ishida, M.; Nakajima, T.; Honda, Y.; Kitao, O.; Nakai, H.; Vreven, T.; Throssell, K.; Montgomery Jr., J. A.; Peralta, J. E.; Ogliaro, F.; Bearpark, M. J.; Heyd, J. J.; Brothers, E. N.; Kudin, K. N.; Staroverov, V. N.; Keith, T. A.; Kobayashi, R.; Normand, J.; Raghavachari, K.; Rendell, A. P.; Burant, J. C.; Iyengar, S. S.; Tomasi, J.; Cossi, M.; Millam, J. M.; Klene, M.; Adamo, C.; Cammi, R.; Ochterski, J. W.; Martin, R. L.; Morokuma, K.; Farkas, O.; Foresman, J. B.; Fox, D. J. Gaussian 16 Rev. B.01; Gaussian Inc.: Wallingford, CT, 2016.
36. Werner, H. J.; Knowles, P. J.; Knizia, G.; Manby, F. R.; Schütz, M. Molpro: a general-purpose quantum chemistry program package. *WIREs Comput Mol Sci* 2012, 2, 242-253.
37. Knowles, P. J.; Hampel, C.; Werner, H. J. Coupled Cluster Theory for High Spin Open Shell Reference Wavefunctions. *J. Chem. Phys.* 1993, 99, 5219-5227.
38. Knowles, P. J.; Werner, H. J. Internally Contracted Multiconfiguration Reference Configuration Interaction Calculations for Excited States. *Theoretica chimica acta* 1992, 84, 95-103.
39. Knowles, P. J.; Andrews, J. S.; Amos, R. D.; Handy, N. C.; Pople, J. A. Restricted Møller--Plesset Theory for Open Shell Molecules. *Chem. Phys. Letters* 1991, 186, 130-136.
40. Amos, R. D.; Andrews, J. S.; Handy, N. C.; Knowles, P. J. Open Shell Møller--Plesset Perturbation Theory. *Chem. Phys. Letters* 1991, 185, 256-264.
41. Knowles, P. J.; Handy, N. C. A Determinant Based Full Configuration Interaction Program. *Computer Physics Communications* 1989, 54, 75-83.
42. Werner, H. J.; Knowles, P. J. An Efficient Internally Contracted Multiconfiguration Reference CI Method. *J. Chem. Phys.* 1988, 89, 5803-5814.
43. Knowles, P. J.; Werner, H. J. An Efficient Method for the Evaluation of Coupling Coefficients in Configuration Interaction Calculations. *Chem. Phys. Letters* 1988, 145, 514-522.
44. Werner, H. J.; Knowles, P. J. A Second Order MCSCF Method with Optimum Convergence. *J. Chem. Phys.* 1985, 82, 5053-5053.
45. Knowles, P. J.; Werner, H. J. An Efficient Second Order MCSCF Method for Long Configuration Expansions. *Chem. Phys. Letters* 1985, 115, 259-267.
46. Knowles, P. J.; Handy, N. C. A New Determinant-based Full Configuration Interaction Method. *Chem. Phys. Letters* 1984, 111, 315-321.
47. Allen, J. W.; Goldsmith, C. F.; Green, W. H. Automatic estimation of pressure-dependent rate coefficients. *Physical Chemistry Chemical Physics* 2012, 14, 1131-1155.
48. Gao, C. W.; Allen, J. W.; Green, W. H.; West, R. H. Reaction Mechanism Generator: Automatic construction of chemical kinetic mechanisms. *Computer Physics Communications* 2016, 203, 212-225.
49. Mebel, A. M.; Georgievskii, Y.; Jasper, A. W.; Klippenstein, S. J. Pressure-dependent rate constants for PAH growth: formation of indene and its conversion to naphthalene. *Faraday Discussions* 2016, 195, 637-670.
50. Jasper, A. W.; Oana, C. M.; Miller, J. A. "Third-Body" collision efficiencies for combustion modeling: Hydrocarbons in atomic and diatomic baths. *Proceedings of the Combustion Institute* 2015, 35, 197-204.
51. Wang, H.; Frenklach, M. Transport properties of polycyclic aromatic hydrocarbons for flame modeling. *Combustion and Flame* 1994, 96, 163-170.
52. Harding, L. B.; Georgievskii, Y.; Klippenstein, S. J. Predictive Theory for Hydrogen Atom-Hydrocarbon Radical Association Kinetics. *The Journal of Physical Chemistry A* 2005, 109, 4646-4656.
53. Ribeiro, J. M.; Mebel, A. M. Reaction mechanism and product branching ratios of the CH + C3H4 reactions: a theoretical study. *Physical Chemistry Chemical Physics* 2017, 19, 14543-14554.
54. Senosiain, J. P.; Miller, J. A. The Reaction of n- and i-C4H5 Radicals with Acetylene. *The Journal of Physical Chemistry A* 2007, 111, 3740-3747.

55. Mebel, A. M.; Georgievskii, Y.; Jasper, A. W.; Klippenstein, S. J. Temperature- and pressure-dependent rate coefficients for the HACA pathways from benzene to naphthalene. Proceedings of the Combustion Institute 2016.
56. Chemical Workbench 4.1.18493; Kintech Lab: Moscow, Russia, 2016.
57. Zádor, J.; Taatjes, C. A.; Fernandes, R. X. Kinetics of elementary reactions in low-temperature autoignition chemistry. *Progress in Energy and Combustion Science* 2011, *37*, 371-421.
58. Knepp, A. M.; Meloni, G.; Jusinski, L. E.; Taatjes, C. A.; Cavallotti, C.; Klippenstein, S. J. Theory, measurements, and modeling of OH and HO<sub>2</sub> formation in the reaction of cyclohexyl radicals with O<sub>2</sub>. *Physical Chemistry Chemical Physics* 2007, *9*, 4315-4331.
59. Estupiñán, E. G.; Smith, J. D.; Tezaki, A.; Klippenstein, S. J.; Taatjes, C. A. Measurements and Modeling of DO<sub>2</sub> Formation in the Reactions of C<sub>2</sub>D<sub>5</sub> and C<sub>3</sub>D<sub>7</sub> Radicals with O<sub>2</sub>. *The Journal of Physical Chemistry A* 2007, *111*, 4015-4030.
60. DeSain, J. D.; Klippenstein, S. J.; Miller, J. A.; Taatjes, C. A. Measurements, Theory, and Modeling of OH Formation in Ethyl + O<sub>2</sub> and Propyl + O<sub>2</sub> Reactions. *The Journal of Physical Chemistry A* 2003, *107*, 4415-4427.
61. Park, J.; Nguyen, H. M. T.; Xu, Z. F.; Lin, M. C. Kinetic Study of the 2-Naphthyl (C<sub>10</sub>H<sub>7</sub>) Radical Reaction with C<sub>2</sub>H<sub>2</sub>. *The Journal of Physical Chemistry A* 2009, *113*, 12199-12206.
62. Mebel, A. M.; Landera, A.; Kaiser, R. I. Formation Mechanisms of Naphthalene and Indene: From the Interstellar Medium to Combustion Flames. *The Journal of Physical Chemistry A* 2017, *121*, 901-926.
63. Middaugh, J. E.; Buras, Z. J.; Matrat, M.; Chu, T.-C.; Kim, Y.-S.; Alecu, I. M.; Vasiliou, A. K.; Goldsmith, C. F.; Green, W. H. A combined photoionization time-of-flight mass spectrometry and laser absorption spectrometry flash photolysis apparatus for simultaneous determination of reaction rates and product branching. *Review of Scientific Instruments* 2018, *89*, 74102.
64. Guan, Q.; Urness, K. N.; Ormond, T. K.; David, D. E.; Barney Ellison, G.; Daily, J. W. The properties of a micro-reactor for the study of the unimolecular decomposition of large molecules. *International Reviews in Physical Chemistry* 2014, *33*, 447-487.
65. Smith, M. C.; Chu, T.-C.; Green, W. H. In 11th U. S. National Combustion Meeting; the Western States Section of the Combustion Institute: Pasadena, California, 2019.

## List of Figures

- Figure 1. C<sub>12</sub>H<sub>9</sub> potential energy surface calculated at the G3(MP2,CC)//B3LYP/6-311G\*\* level of theory. Newly added species and pathways are marked in red. Energies are relative to 2-Naphthalenyl radical + C<sub>2</sub>H<sub>2</sub>. ..... 4
- Figure 2. C<sub>14</sub>H<sub>11</sub> potential energy surface calculated at the G3(MP2,CC)//B3LYP/6-311G\*\* level of theory, starting from 1-N<sub>2</sub>, 1-N<sub>7</sub>, and 1-N<sub>11</sub> isomers reacting with C<sub>2</sub>H<sub>2</sub>. Energies are relative to 2-Naphthalenyl radical + 2C<sub>2</sub>H<sub>2</sub>. ..... 5
- Figure 3. C<sub>14</sub>H<sub>11</sub> potential energy surface calculated at the G3(MP2,CC)//B3LYP/6-311G\*\* level of theory, starting from 2-N<sub>2</sub>, 2-N<sub>8</sub>, and 2-N<sub>11</sub> isomers reacting with C<sub>2</sub>H<sub>2</sub>. Newly added species and pathways are marked in red. Energies are relative to 2-Naphthalenyl radical + 2C<sub>2</sub>H<sub>2</sub>. ..... 5
- Figure 4. C<sub>14</sub>H<sub>9</sub> potential energy surface calculated at the G3(MP2,CC)//B3LYP/6-311G\*\* level of theory, starting from N1-CS38, N1-CS39, N1-CS40, and N1-CS41 isomers reacting with C<sub>2</sub>H<sub>2</sub>. Energies are relative to N1-CS38 + C<sub>2</sub>H<sub>2</sub>. ..... 7
- Figure 5. Important elementary reactions connecting 1-C<sub>10</sub>H<sub>7</sub> + C<sub>2</sub>H<sub>2</sub> and 2-C<sub>10</sub>H<sub>7</sub> + C<sub>2</sub>H<sub>2</sub> networks. The energy of species is given relative to 2-C<sub>10</sub>H<sub>7</sub> + C<sub>2</sub>H<sub>2</sub> in kcal/mol, and the energy of each TS is shown next to the corresponding arrow. .... 9

Figure 6. H-abstraction reactions calculated at the G3(MP2,CC)//B3LYP/6-311G** level of theory and included in the naphthalenyl HACA model. ....	13
Figure 7. Simulated species concentration profiles starting from 1-C <sub>10</sub> H <sub>7</sub> + C <sub>2</sub> H <sub>2</sub> . (a) 30 Torr, 800 K, (b) 300 Torr, 800 K, (c) 30 Torr, 1500 K, (d) 300 Torr, 1500 K. ....	14
Figure 8. Important pathways and ROP analysis of 1-C <sub>10</sub> H <sub>7</sub> + C <sub>2</sub> H <sub>2</sub> at 1500 K. ROP values are the percentages of reactants converted into products, and evaluated at t = 1e-6 sec. The values in blue are for 30 Torr, and red for 300 Torr. ....	16
Figure 9. Simulated species concentration profiles starting from 2-C <sub>10</sub> H <sub>7</sub> + C <sub>2</sub> H <sub>2</sub> . (a) 30 Torr, 800 K, (b) 300 Torr, 800 K, (c) 30 Torr, 1200 K, (d) 300 Torr, 1200 K. ....	18
Figure 10. Important pathways and ROP analysis of 2-C <sub>10</sub> H <sub>7</sub> + C <sub>2</sub> H <sub>2</sub> at 1500 K. ROP values are the percentages of reactants converted into products, and evaluated at t = 1e-6 sec. The values in blue are for 30 Torr, and red for 300 Torr. ....	19

#### List of Tables

Table 1. Pressure-dependent rate coefficients of important reactions in ACN formation from 2-naphthalenyl + C <sub>2</sub> H <sub>2</sub> on the C <sub>12</sub> H <sub>9</sub> PES. ....	10
Table 2. Reaction rate parameters of the H-abstraction reactions calculated in this work in the form of $AT^n \exp(-E/RT)$ ; the units are cm <sup>3</sup> mol <sup>-1</sup> s <sup>-1</sup> and kcal/mol. ....	11